Investigation of lithium and fluorine content in geological materials using Nuclear Reaction Analysis (NRA)

de La Rosa, Nathaly

2019

Document Version:
Publisher's PDF, also known as Version of record

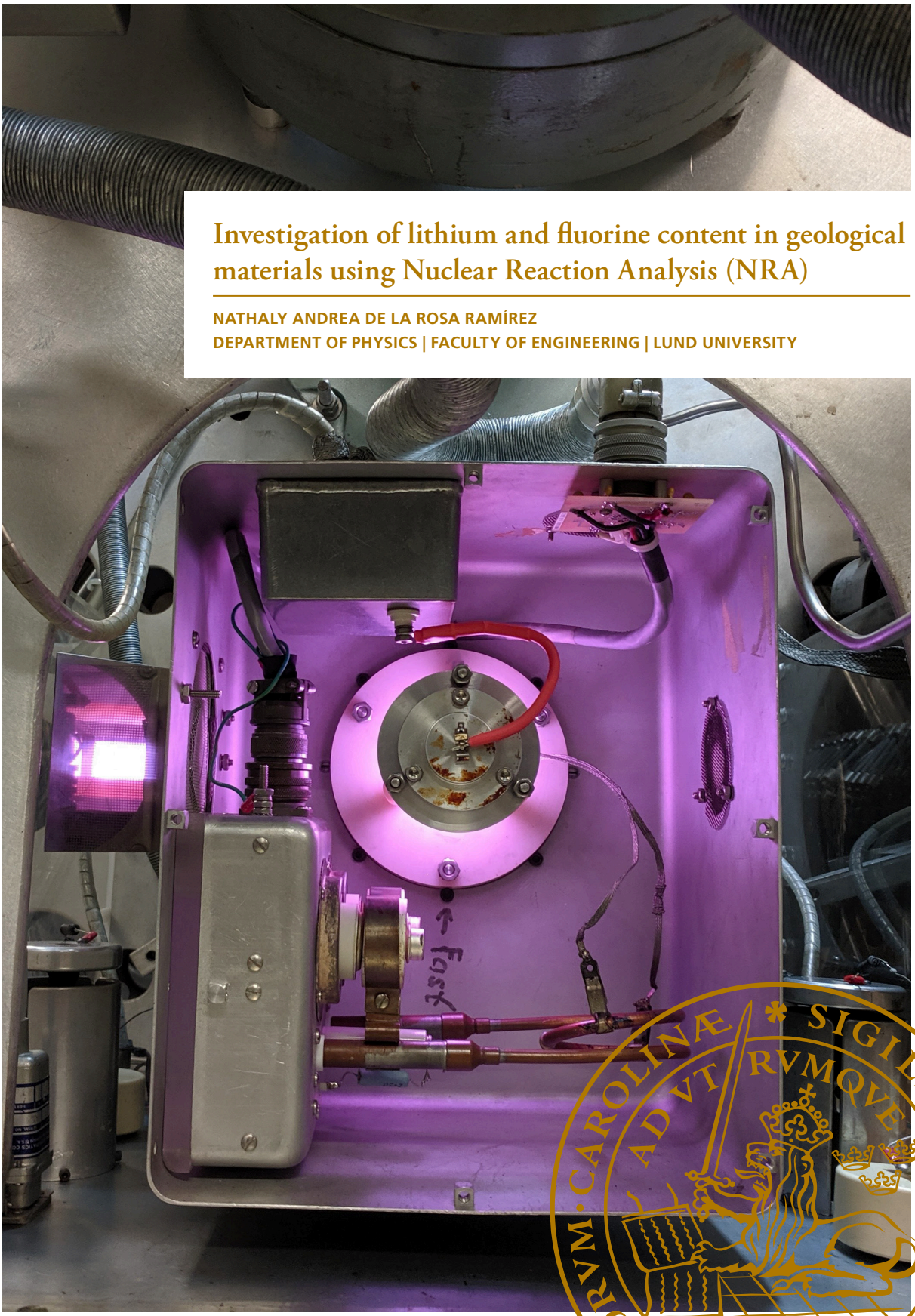

Investigation of lithium and fluorine content in geological materials using Nuclear Reaction Analysis (NRA)

NATHALY ANDREA DE LA ROSA RAMÍREZ
DEPARTMENT OF PHYSICS | FACULTY OF ENGINEERING | LUND UNIVERSITY

This thesis deals with the optimization of the Nuclear Reaction Analysis (NRA) technique to determine the content of lithium and fluorine in geological materials. Measuring low concentrations of these isotopes is of great relevance in many fields. NRA is part of a big family of analysis techniques known as Ion Beam Analysis, which are non-destructive, short in measurement time, and have very good sensitivity over the hole periodic table. If you open this book, you can read about this incredible way of measuring lithium and fluorine concentrations as low as tens of parts per million.

Printed by Media-Tryck, Lund 2019 NORDIC SWAN ECOLABEL 3041 0903

LUND UNIVERSITY

Lund University
Faculty of Engineering
Division of Nuclear Physics

ISBN 978-91-7895-219-9 print
978-91-7895-220-5 pdf

INVESTIGATION OF LITHIUM AND FLUORINE CONTENT IN GEOLOGICAL MATERIALS USING NUCLEAR REACTION ANALYSIS (NRA)

INVESTIGATION OF LITHIUM AND FLUORINE CONTENT IN GEOLOGICAL MATERIALS USING NUCLEAR REACTION ANALYSIS (NRA)

by

NATHALY ANDREA DE LA ROSA RAMÍREZ

LUND
UNIVERSITY

Thesis for the degree of Doctor of Philosophy in Engineering

Opponent: Dr. Patrick Reichart
Institut LRT2
Universität der Bündeswehr München
Werner-Heisenberg-Weg 39
85577 Neubiberg, Germany

To be presented, with the permission of the Faculty of Engineering at Lund University, for public criticism on Friday, 15th of November 2019 at 13:15 in the Rydberg hall at the Department of Physics, Professorsgatan 1, Lund.

Organization	Document name
LUND UNIVERSITY Department of Physics Professorsgatan 1, Lund	**DOCTORAL DISSERTATION** Date of disputation 2019-11-15 Sponsoring organization
Author(s) Nathaly Andrea De La Rosa Ramírez	

Title and subtitle

Investigation of lithium and fluorine content in geological materials using Nuclear Reaction Analysis (NRA)

Abstract

This work focuses on the optimization of the Nuclear Reaction Analysis (NRA) technique to determine the content of lithium and fluorine in geological materials. Measuring low concentration of these isotopes is of great relevance in many fields such as geological, astrophysical, biological and material sciences.

Light elements as lithium and fluorine are considered as geochemical tracers in various geological processes such as the crust-mantle recycling. In these applications, precise measurements are required. Our interest in geological applications is part of an interdisciplinary collaboration with geologists who provide us with samples and are interested in our results. The development of this project has enabled the Lund Ion Beam Analysis Facility (LIBAF) group to establish a technique for lithium and fluorine measurements that can be used in many fields.

NRA is part of a family of analysis techniques known as Ion Beam Analysis (IBA). The advantages offered by IBA techniques are non-destructiveness, short measurement time, and very good sensitivity over the hole periodic table. Equipment such as particle accelerators and radiation detectors are needed to carry out IBA techniques. These types of equipment have been utilized at the LIBAF in order to perform NRA using Li-bearing and F-bearing materials. In NRA, the samples are scanned by energetic ions such as protons or deuterons to induce reactions with the sample elements. Many reactions can take place producing charged particles, X-rays and gamma rays. The ^{7}Li(p,α)^{4}He and ^{19}F(p, α)^{16}O reactions were utilized to obtain lithium and fluorine detection limits below 1 ppm and 50 ppm respectively.

Key words

Ion Beam Analysis, Elemental composition, Accelerator, Nuclear Reaction Analysis

Classification system and/or index terms (if any)

Supplementary bibliographical information	Language
	English
ISSN and key title	ISBN
	978-91-7895-219-9 print 978-91-7895-220-5 pdf
Recipient's notes	Number of pages: 119 / Price
	Security classification

INVESTIGATION OF LITHIUM AND FLUORINE CONTENT IN GEOLOGICAL MATERIALS USING NUCLEAR REACTION ANALYSIS (NRA)

by

NATHALY ANDREA DE LA ROSA RAMÍREZ

LUND
UNIVERSITY

A doctoral thesis at a university in Sweden takes either the form of a single, cohesive research study (monograph) or a summary of research papers (compilation thesis), which the doctoral student has written alone or together with one or several other author(s).

In the latter case the thesis consists of two parts. An introductory text puts the research work into context and summarizes the main points of the papers. Then, the research publications themselves are reproduced, together with a description of the individual contributions of the authors. The research papers may either have been already published or are manuscripts at various stages (in press, submitted, or in draft).

Cover illustration front: Radio frequency ion source, the heart of the accelerator at LIBAF
Cover illustration back: Nathaly at LIBAF, picture by Mikael Elfman

Division of Nuclear Physics
Department of Physics
Lund University
Box 118
SE-221 00 Lund
Sweden

ISBN: 978-91-7895-219-9(print)
ISBN: 978-91-7895-220-5(pdf)

Powered by LaTeX
Printed in Sweden by Media-Tryck, Lund University, Lund 2019

Dedicated to Alba and Jorge

ABSTRACT

This work focuses on the optimization of the Nuclear Reaction Analysis (NRA) technique to determine the content of lithium and fluorine in geological materials. Measuring low concentration of these isotopes is of great relevance in many fields such as geological, astrophysical, biological and material sciences.

Light elements as lithium and fluorine are considered as geochemical tracers in various geological processes such as the crust-mantle recycling. In these applications, precise measurements are required. Our interest in geological applications is part of an interdisciplinary collaboration with geologists who provide us with samples and are interested in our results. The development of this project has enabled the Lund Ion Beam Analysis Facility (LIBAF) group to establish a technique for lithium and fluorine measurements that can be used in many fields.

NRA is part of a family of analysis techniques known as Ion Beam Analysis (IBA). The advantages offered by IBA techniques are non-destructiveness, short measurement time, and very good sensitivity over the hole periodic table. Equipment such as particle accelerators and radiation detectors are needed to carry out IBA techniques. These types of equipment have been utilized at the LIBAF in order to perform NRA using Li-bearing and F-bearing materials. In NRA, the samples are scanned by energetic ions such as protons or deuterons to induce reactions with the sample elements. Many reactions can take place producing charged particles, X-rays and gamma rays. The ^{7}Li(p,α)^{4}He and ^{19}F(p, α)^{16}O reactions were utilized to obtain lithium and fluorine detection limits below 1 ppm and 50 ppm respectively.

POPULAR SUMMARY

If you would like to prepare a wedding cake, you would probably follow a recipe that tells you the ingredients and the instructions for it. But, what if you are curious about someone else's wedding cake recipe. Surely we cannot just cut a piece, most certainly not before the party. So, how can we find out the ingredients and the recipe?

One could start by staring (awkwardly) at the cake, distinguishing its colors and textures. Say the cake looks black, you may first guess that the cake contains chocolate, but, does it? and if so, how much? What if the cake is not black? And what about the rest of the ingredients? What if the cake also has small chunks of something? One could imagine the cake containing raisins or almonds but then again, which one is it and how many? And what about the aroma? What is it that you smell? Is that vanilla? Lemon? We better make sure, some of those ingredients mix better than others.

For sure, at some point you may be able to take a bite of the cake (probably with your eyes closed to be focused) and try to compare the taste of the cake with all the flavors and textures that you know. Now, we can start distinguishing perhaps the usual ingredients: flour, eggs, butter and milk, and so on. But the real question here is, in which proportion are they mixed? And what about that extra something that makes this cake so unique? How do we scrutinize the cake without destroying it?

The work carried out in this thesis can be imagined as similar to the challenge of knowing the exact quantity of ingredients that the cake has. Except that the cake is an odorless tiny rock sample the size of a grain of sugar, and that you are not supposed to eat rocks! Even if you did, our senses of sight, smell and taste would unfortunately not lead us adequately to find the recipe of the rock/cake. So, how do we go about that?

We know that the ingredients of a rock sample are atoms, actually a huge number of them, and we want to be able to know their quantities and their distribution inside the sample. We also know that an atom is composed by an atomic nucleus and orbiting electrons. The atomic nucleus is composed of protons and neutrons. The number of protons defines what element in the periodic table it is, and the number of neutrons does not affect its chemical properties. Atoms of the same element with different number of neutrons are called isotopes.

To determine the number of certain atoms that a rock sample has, we take the sample to the laboratory and expose it to a beam of charged atoms (called ions) and measure the outcome of the interaction between the beam and the sample. Being more precise about this, what we measure is the result of the interactions between the atomic nuclei of the beam and the nuclei sample atoms. These interactions are called nuclear reactions.

Given that the nuclear reactions occur only between one atom of the beam and just one atom of the sample, it is rather straightforward to infer which atoms are in the sample and how many of them there are, by measuring the number of reaction products (the outcomes). As a matter of fact we can distinguish not only different chemical elements but also different isotopes. By correlating the reaction products with the place where the sample was hit by the beam we can create a photo of how the different elements and isotopes are distributed. It is like being able to know the exact composition of the different layers in the cake without ever biting into it!

So, coming back to the rocks with the size of a grain of sugar, what is it that we want to study about them? The answer is the quantity of lithium and fluorine isotopes in them. With the technique used in this work, it is possible to distinguish 1 atom of lithium or fluorine in 1 million of other atoms. Their exact quantities and distribution of isotopes are of great relevance in many areas of knowledge such as geology, medicine, material and forensic sciences, etc.

In the end, we do not figure out the exact recipe for the rock/cake, but we are able to determine its ingredients with great precision and for sure this is an excellent start.

POPULÄRVETENSKAPLIG SAMMANFATTNING PÅ SVENSKA

Om du skulle vilja baka en bröllopstårta, skulle du troligtvis följa ett recept med ingredienser och instruktioner. Men om du skulle vara nyfiken på någon annans bröllopstårta, vad gör du då? Vi kan så klart inte bara skära upp en bit, i synnerhet inte innan festen! Hur kan vi då ta reda på ingredienserna och receptet?

Man skulle kunna börja med att titta på tårtan och notera dess färger och texturer. Om tårtan är svart, kanske du gissar att den innehåller choklad. Men gör den verkligen det? Och hur mycket? Och om tårtan nu inte är svart? Vilka andra ingredienser innehåller den? Tänk om tårtan innehåller små bitar av något, kanske russin eller mandlar? Men vilket är det, och hur många? Och hur är det med aromen? Vad är det du luktar? Är det vanilj? Citron? Vi måste vara noggranna för vissa smakkombination är bättre än andra.

Säkerligen får du så småningom ta en bit av tårtan (med ögonen stängda för att kunna fokusera) och då kan du jämföra tårtans smak med alla smaker och texturer som du känner till. Nu kan vi kanske urskilja de vanliga ingredienserna: mjöl, ägg, smör, mjölk och så vidare. Men den viktiga frågan är i vilka proportioner ingredienserna blandats. Och vad är det där extra, som gör just den här tårtan så unikt god? Hur kan vi detaljundersöka tårtan utan att förstöra den?

Arbetet som beskrivs i denna avhandling påminner om utmaningen i att ta reda på de exakta kvantiteterna av olika ingredienser som finns i tårtan. Skillnaden är bara att tårtan istället är ett luktlöst pyttelitet mineralprov som är ungefär lika stort som ett sockerkorn, och att du inte bör äta stenar! Även om du nu skulle försöka smaka på stenen, skulle varken lukt eller smak - eller för den delen din syn – leda till kunskap om receptet för stenen/tårtan. Så hur gör vi då?

Vi vet att ingredienserna i ett mineralprov är atomer, faktiskt ett otroligt stort antal av dem, och vi vill ta reda på deras kvantiteter och distribution inne i provet. Vi vet också att en atom består av en atomkärna med omgivande elektroner. Atomkärnan består i sin tur av protoner och neutroner. Antalet protoner definierar vilket kemiskt grundämne det är, och neutronerna påverkar inte de kemiska egenskaperna. Atomer av samma grundämne med olika antal neutroner kallas för isotoper.

För att betsämma antalet av en viss typ av atomer i ett mineralprov, tar vi provet till laboratoriet och låter det träffas av en stråle av laddade atomer (kallade joner) och mäter resultatet av interaktionerna mellan strålen och provet. Mer precist uttryckt mäter vi resultatet av interaktionerna mellan atomkärnor i strålen och atomkärnor i provet. Dessa interaktioner kallas för kärnreaktioner.

Om vi antar att kärnreaktioner sker bara mellan en enda atom i strålen och en enda atom i provet, är det någorlunda enkelt att räkna ut vilka slags atomer, och hur många av dem, som finns i provet genom att mäta reaktionsprodukterna som bildas. Vi kan faktiskt skilja mellan inte bara olika grundämnen utan också olika isotoper. Genom att studera vilka reaktionsprodukter som bildas när strålen träffar olika delar av provet kan vi skapa en bild av hur de olika grundämnena och deras isotoper är fördelade. Det är som att ta reda på exakt vad varje lager i en tårta innehåller utan att ens röra den!

Vi återgår till mineralproverna som är så små som sockerkorn. Vad är det egentligen vi vill veta om dem? Svaret är att vi vill veta hur mycket litium- och flourisotoper det finns i dem. Men den teknik som beskrivs här, är det möjligt att urskilja en enda atom av litium eller flour bland en miljon andra atomer. Den exakta mängden och fördelningen av isotoper är viktig för många olika forskningsfält, såsom geologi, medicin, materialvetenskap, rättsmedicin med mera.

Vi kan inte få reda på det exakta receptet för hur stenen/tårtan har blivit till, men vi kan bestämma ingredienserna med otrolig precision. Det är en utmärkt start!

RESUMEN EJECUTIVO

Si quisieras preparar un pastel de bodas, probablemente seguirías una receta para saber los ingredientes y las instrucciones. Pero, ¿ qué pasaría si estuvieras en una fiesta de matrimonio y quisieras saber la receta exacta del pastel? Seguramente no cortatrías un pedazo de pastel, y nunca antes de que la pareja lo parta. Entonces, ¿cómo podríamos encontrar la receta?

Uno podría comenzar fijándose (incómodamente) en el pastel, distinguiendo sus colores y texturas. Digamos que el pastel se ve oscuro, tu podrias suponer que el pastel contiene chocolate, pero, ¿ si sería cierto? y si lo es, ¿cuánto chocolate tiene? Qué tal si el pastel no es oscuro, ¿qué otros ingredientes tendría? Qué tal si el pastel también tiene trozos de algo? Uno podría imaginar que se trata de uvas pasas o almendras, pero una vez más, ¿cuál de las dos y en qué cantidad? ¿Y qué decir del olor?, ¿huele a vainilla o a limón? Debemos asegurarnos bien, varios de esos ingredientes combinan mejor que otros.

Seguramente, en algún momento vas a poder probar el pastel (probablemente con los ojos cerrados para poderte concentrar) y tratar de comparar el sabor del pastel con todos los sabores y texturas que puedas recordar. Entonces, podemos comenzar quizas distinguiendo los sabores usuales: harina, huevo, mantequilla, leche, entre otros. Pero la verdadera pregunta acá es, ¿en qué proporción están mezclados? ¿Y qué tal la pizca que hace a este pastel tan especial? ¿Cómo podemos escrutiñar el pastel sin destruirlo?

Se podría pensar que el trabajo realizado en esta tesis es equivalente al reto de conocer la cantidad exacta de los ingredientes en el pastel de bodas. Excepto que en nuestro caso, el pastel es un pequeña roca sin olor alguno, del tamaño de un grano de azucar y que no se puede comer! Bueno, aunque quisíeramos comernos una pedazo de la roca, nuestro sentidos del gusto desafortunadamente no nos llevaría correctamente a encontrar la receta de la roca/pastel. Entonces, ¿qué podríamos hacer?

Nosotros sabemos que los ingredientes de una roca son átomos, de hecho, un número enorme de ellos, entonces queremos ser capaces de conocer el número y la distribución de ellos en la muestra. Támbien sabemos que un átomo está compuesto por el núcleo atómico, y los electrones que lo orbitan. El núcleo atómico está compuesto por protones y neutrones. El número de protones define qué elemento es en la tabla periódica, y el número de neutrones no

afecta sus propiedades químicas. Átomos de un mismo elemento con diferente número de protones se llaman isótopos.

Para determinar el número de ciertos átomos que una roca tiene, tomamos una pequeña muestra y la llevamos al laboratorio para exponerla a un haz de átomos cargados (llamados iones), y medimos el resultado de la interacción entre los núcleos atómicos del haz y los núcleos atómicos de la muestra. Estas interacciones se llaman reacciones nucleares.

Dado que las reacciones nucleares occurren únicamente entre un átomo del haz y un átomo de la muestra, es relativamente directo inferir que átomos y cuántos están presentes en la muestra al medir el número de los productos de las reacciones (los resultantes). De hecho, podemos distinguir no solo los elementos químicos, sino también sus diferentes isótopos. Dado que una muestra puede ser escaneada con el haz, de la relación entre los productos de la reacción con el la posicion del haz en la muestra podemos crear una imaagen de cómo los diferentes elementos e isotopos están distibuidos. Es como poder saber la composición exacta de las diferentes capas del pastel sin haberlo mordido jamás!

Entonces, volviendo a las rocas del tamaño de un grano de azucar, ¿qué es lo que queremos estudiar de ellas? La respuesta es la cantidad de isotopos de litio y fluor en ellas. Con la técnica usada en este trabajo es posible distinguir un átomo de litio o fluor de entre un millón de otros átomos. Las cantidades exactas y la distribución de estos isotopos son de muy alta relevancia en muchas áreas del conocimiento como en geología, medicina, y ciencias de los materiales, ciencias forences, entre otras.

Así que al final no logramos obtener la receta exacta de nuestra roca/pastel, pero podemos determinar sus ingredientes con excelente precisión y esto de seguro es un gran comienzo.

CONTENTS

LIST OF FIGURES

LIST OF PUBLICATIONS

I **Lithium analysis using a double-sided silicon strip detector at LIBAF.**

Nucl. Intr. and Meth. B 404 (2017) 29-33.

N. De La Rosa, P. Kristiansson, E. J. C. Nilsson, L. Ros, M. Elfman, J. Pallon.

I analyzed the data and wrote the article.

II **Quantification of lithium at ppm level in geological samples using nuclear reaction analysis.**

J Radioanal Nucl Chem. (2018) 317(1) 253-259.

N. De La Rosa, P. Kristiansson, E. J. C. Nilsson, L. Ros, J. Pallon, H. Skogby.

I helped to prepare and conduct the experiment. I was in charge of the data analysis and writing the article.

III **Automating the setup and control of the pre-sample charge measurement system at the Lund Ion-beam Analysis Facility**

J.W. R. Frost, **N. De La Rosa**, P. Kristiansson, J. Pallon.

Manuscript submitted to Nucl. Intr. and Meth.

I took part in conducting the experiment and analysing the data. I helped writing the article.

IV **Ion beam analysis of fluorine in geological samples.**

N. De La Rosa, J.W. R. Frost, E. J. C. Nilsson, J. Pallon, M. Elfman.

Manuscript in preparation.

I prepared and conducted the experiment. I analyzed the data and wrote the article.

OTHER PUBLICATIONS NOT INCLUDED IN THIS THESIS

I **A nuclear geochemical analysis system for boron quantification using a focused ion beam**

E. J. C. Nilsson, P. Kristiansson, **N. De La Rosa**, M. Elfman, U. Hålenius J. Pallon, H. Skogby.

J Radioanal Nucl Chem. 311(1) (2017) 355-364.

II **A new quantitative X-ray system for micro-PIXE analysis**

J. Pallon, **N. De La Rosa**, M. Elfman, P. Kristiansson, E. J. C. Nilsson, L. Ros.

X-Ray Spectrometry, 46(5)(2017) 319-324.

III **Late magmatic controls on the origin of schorlitic and foititic tourmalines from late-Variscan peraluminous granites of the Arbus pluton (SW Sardinia, Italy): Crystal-chemical study and petrological constraints**

F. Bosi, S. Naitza, H. Skogby, F. Secchi, A. M. Conte, S. Cuccuru, U. Hålenius, **N. De La Rosa**, P. Kristiansson, E. J. C. Nilsson, L. Ros, G.B. Andreozzi

Lithos, 308-309 (2018) 395-411.

LIST OF PARTICIPATION AT CONFERENCES

Poster: **Lithium analysis using a double-sided silicon strip detector at LIBAF**

N. De La Rosa, P. Kristiansson, E. J. C. Nilsson, L. Ros, M. Elfman, J. Pallon.

15^{th} International Conference on Nuclear Microprobe Technology and Applications (ICNMTA) 2016.

Poster: **Trace concentration of Lithium Measured by NRA in Geological samples**

N. De La Rosa, P. Kristiansson, E. J. C. Nilsson, L. Ros, M. Elfman, J. Pallon.

23^{th} International Conference on Ion Beam Analysis (IBA) 2017.

Talk: **Quantitative determination of fluorine using a double-sided silicon strip detector**

N. De La Rosa, P. Kristiansson, E. J. C. Nilsson, M. Elfman, J. Pallon.

16^{th} International Conference on Nuclear Microprobe Technology and Applications (ICNMTA) 2018.

Talk: **Quantitative determination of fluorine at LIBAF**

N. De La Rosa, P. Kristiansson, E. J. C. Nilsson, M. Elfman, J. Pallon.

Swedish nuclear physics meeting XXXVIII 2018.

Part I

RESEARCH CONTEXT

1

INTRODUCTION

Quantification of light elements such as lithium and fluorine in geological materials is at the heart of understanding their genesis and physico-chemical history. The relevance of measuring light elements in minerals led to the establishment of a program driven by a collaboration between geologists from the Swedish Museum of Natural History and the Lund Ion Beam Analysis Facility (LIBAF) group [16]. Within the framework of this program at LIBAF, hydrogen isotopes [17, 18], oxygen [19] and boron [20, 21] analysis has been performed using Ion Beam Analysis (IBA) techniques. In order to continue expanding the capabilities of measuring light elements, this PhD thesis focuses on techniques for assessing the concentration of lithium isotopes and fluorine in minerals using IBA.

Lithium and fluorine are considered of great importance in medicine [22, 23], as well as material science [24, 25]. In geology or Earth science, lithium and fluorine are quantified in minerals to study the origin of volatile elements on Earth and the solar system [26, 27], and the crust-mantle recycling process [28]. In these investigations, measuring traces of fluorine or isotopes of lithium helps to understand physico-chemical processes that rocks undergo in their formation and correlate this to the geological history of the surroundings region [29]. Traces of light elements for geological applications can be quantified to very low levels using IBA techniques. Within these techniques, Nuclear Reaction Analysis (NRA) is the technique proposed in this work to determine quantitatively lithium and fluorine.

IBA has been demonstrated to be a suitable method to investigate the composition and distribution of light and heavy elements at very low concentration ($<$ 1 ppm) in geological materials [30]. IBA utilizes nano-and micro-sized ion beams of 1 MeV-5 MeV as probes [31]. At these energies the ions initiate processes at the atomic and nuclear level that provide information on the elemental content of a specimen over a wide range of the periodic table. When a sample contains lithium and fluorine, these elements interact with ions at the nuclear level, initiating reactions of which products can be charged particles, neutrons and γ rays. In this work, the quantification of reaction products, from the interactions of fluorine and lithium with light ion beams such as proton and deuterium beams, enabled the determination of the concentration of lithium and fluorine in the samples.

The overall structure of this thesis takes the form of six chapters, in addition to two articles already published and two manuscripts. Chapter 2 begins by laying out the theoretical dimensions of the research, which are related to the principles of IBA and the basic interactions of the ions with the matter. Chapter 2 closes by comparing IBA with other analytical techniques. Chapter 3 is concerned with the equipment and methodology used for this study. Chapters 4 and 5 proceed to describe the Ion Beam Analysis of lithium and fluorine respectively, as carried out at the LIBAF. The final chapter offers concluding remarks. The content related to the quantitative determination of ^{7}Li was part of my Licentiate work titled "Nuclear Reaction Analysis in Li-bearing samples" [32].

2

ION BEAM ANALYSIS (IBA) METHODS

Ion beam analysis is a multi-elemental technique, the principle of which is to interact energetic ions interact with matter in order to induce radiation emission. Through the analysis of the emitted radiation, the structure and elemental composition of matter can be found. The interaction of ions with matter depends on parameters such as the energy and mass of the ion and the atomic and mass number of the matter. Energetic ions can be $^{1}H^{+}$, protons, or $^{2}H^{+}$, deuterons, of a few MeV which initiate atomic and nuclear processes, see Fig 2.1. Within these processes, there are three mechanisms which are of primary interest for this work, nuclear reaction analysis (NRA), particle-induced X-ray emission (PIXE) and elastic (Rutherford) backscattering (RBS). These techniques are used to derive information on the elemental content of a specimen over the whole periodic table. For instance, PIXE helps with the determination of the composition for elements ranging from Na to U [33], while NRA advantageously expands the range to lighter elements such as Be, B, Li, and F [34]. RBS is very popular in material analysis since it has been used extensively to determine the distribution of target elements with Z>10 as a function of depth in thin films [31]. This chapter describes the fundamental physics of RBS, PIXE and NRA techniques and shows how these techniques were suitable for this work. Furthermore, a brief description about energy loss by ions passing through matter and a comparison of IBA with other techniques are also included.

2.1 ELASTIC OR RUTHERFORD BACKSCATTERING (RBS)

The Elastic backscattering technique provides information about the elemental area density and the stoichiometry in the near surface region of thin films and bulk materials with a resolution of 10 nm-30 nm [10]. RBS is a nondestructive and fast technique that does not require reference standard samples to determine quantitative analysis since the Coulomb scattering cross section can be independently calculated.

By the use of RBS the target atom mass is determined from the energy of the backscattered projectile (E_1) and its initial energy (E_0) [29]. Both energies are measurable and can be theoretically related to the projectile and target nucleus masses through kinematic equations deduced from momentum conservation.

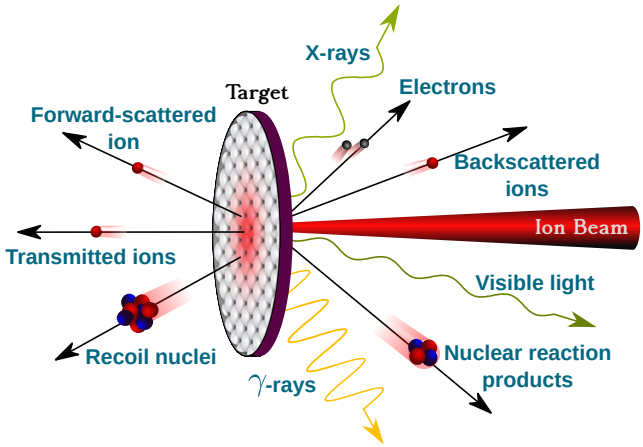

Figure 2.1: Schematic diagram of possible reaction products by an ion beam of MeV energy range.

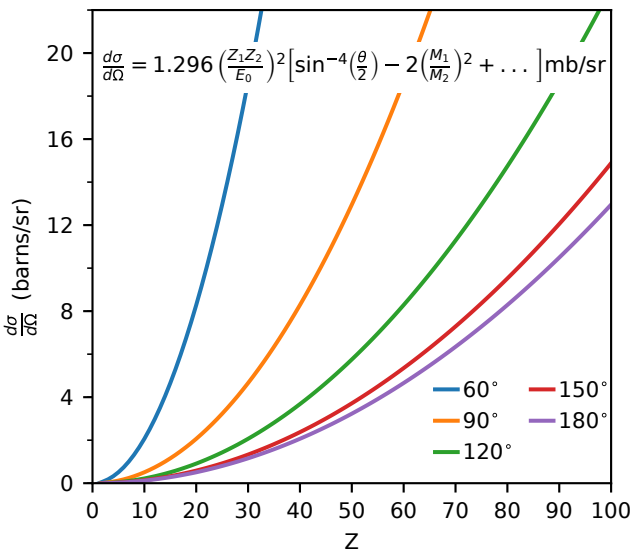

Figure 2.2: According to the laboratory differential cross section function $\left(\frac{d\sigma}{d\Omega}\right)$, particles of mass M_1, charge $Z_1 e$ and incident energy E_0 (MeV) are scattered at θ° by a target consisting of particles of mass M_2 and charge $Z_2 e$. The plot shows curves of the differential cross section at different angles for elastic scattering of 2-MeV α particles for various targets with atomic number Z from 1 to 100.

Elastic scattering takes place when ions interact with target nuclei at energies that do not exceed the Coulomb barrier. The incident ion beam energy is

typically 200 keV-400 keV for protons or 1 MeV-3 MeV for α particles [35]. The elastic scattering cross-section at a certain angle θ depends on the initial energy of the ion beam E_0, the atomic number and mass of the ion beam and the target. Fig 2.2 illustrates the cross sections for 1-MeV protons scattered by various targets with different Z values at different angles. These curves indicate that cross sections are higher for high Z targets. For light elements, the differential cross sections at backward angles are in the 1 mb/sr to 100 mb/sr range. This implies that RBS is comparatively not suitable to quantify lithium or fluorine. However, in this work RBS was utilized to obtain previews of samples, that provided a guide to localize a zone of interest within the samples to be scanned by the beam. Fig.2.3 displays a $LiAl(Si_4O_{10})$ image and a 2D backscattered protons distribution map of the mineral. The mineral was bombarded by protons with an initial energy of 1 MeV.

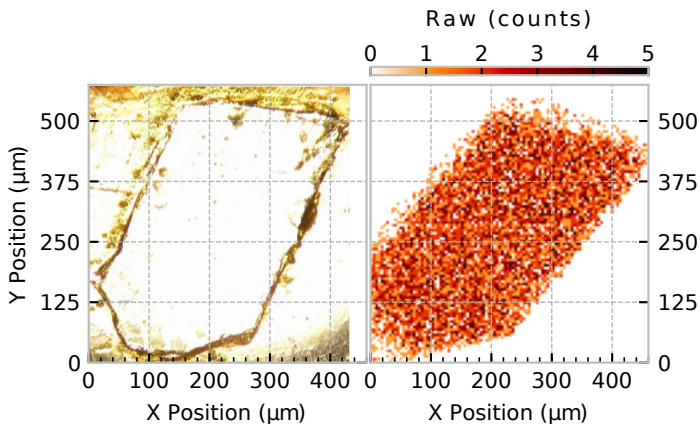

Figure 2.3: Image of a $LiAl(Si_4O_{10})$ mineral (left) and its respective 2D backscattered protons distribution map (right). The mineral was scanned with a proton beam at 1 MeV.

2.2 PARTICLE INDUCED X-RAY EMISSION (PIXE)

This technique categorizes materials by measuring X-rays emitted in the deexcitation of atomic electrons in a specimen, which is irradiated by accelerated charged particles [33]. The X-ray energies allow for the identification of elements from which the electronic deexitation takes place. Fig. 2.4 shows a typical PIXE spectrum measured when a proton beam at 850 keV irradiated a standard reference sample (NIST 610 sample [1]). Based on the X-ray energies, elements from silicon to gallium have been identified. A schematic illustration

of the interaction between an energetic proton and sample atomic electrons with the subsequent X-ray emission is also shown as inset in Fig. 2.4.

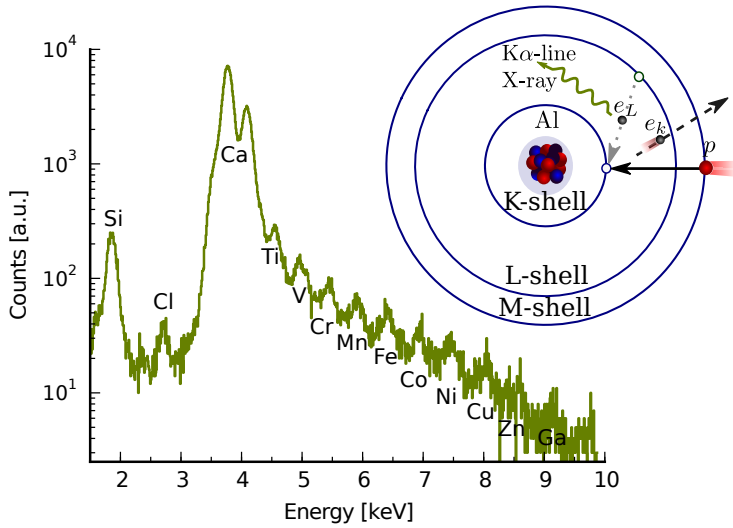

Figure 2.4: Energy spectrum of characteristic X-rays from a standard reference sample (NIST 610 [1]). This spectrum was obtained simultaneously with the spectrum shown in Fig 4.3. The inset illustrates the emission of a characteristic X-ray by a target atom, subsequent to an inner-shell ionization.

PIXE, as all IBA techniques, is a powerful non-destructive elemental analysis method widely used in cultural heritage study, geology, archaeology and other fields to investigate provenience, dating and authenticity. PIXE offers a sensitivity of the order of 0.1 ppm to 1 ppm for elements with Z > 12 [36]. Unfortunately PIXE is not as useful for quantifying elements with Z <12. This is due to the characteristic K_α X-rays of elements from hydrogen to about sodium have energies below 1 keV, which are absorbed in any surface dead layer of a detector [31]. The quantitative determination of elements with Z <12 is possible using NRA

In Paper II, PIXE was used as a complementary technique combined with NRA. The equipment and method implemented to carry out NRA and PIXE simultaneously are described in Chapter 4.

2.3 NUCLEAR REACTION ANALYSIS (NRA)

The NRA technique is concerned with determining the elemental composition of matter through the quantification of the reaction products coming from

reactions induced by ion beams. The incident ions should have sufficient energy to overcome the Coulomb barrier from the target nuclei, and interact with matter within the energy regime of the attractive nuclear force [10]. A useful estimate of the Coulomb barrier height is [29],

$$E = \frac{zZ}{a^{1/3} + A^{1/3}} \,\mathrm{MeV} \tag{1}$$

where a and A are the atomic numbers of the projectile and the target nuclei respectively, and z and Z are their atomic numbers. The barrier height becomes greater as the atomic number of the target nucleus increases. In practice, light incident ions such as p, d, ^3He and ^4He of energies up to 4 MeV will only induce reactions with significant rates in target atoms with Z up 20. Therefore, NRA is a good technique for light elements of Z$<$ 20.

2.3.1 *Principles of nuclear reactions*

Nuclear reactions can take place when two particles or nuclei, a and A, interact to produce, $B + b$. A condensed manner of referring to the reaction is $A(a, b)B$, where a is the projectile or energetic ion (from an accelerator, reactor or radioactive source), A is a stationary target nucleus, b is the ejected particle (that can be a light nuclei or radiation), and B is the recoil nuclei, that usually is a heavy nucleus stopped in the bulk target [37].

The reaction product is specific to a particular isotope of an element, since nuclear characteristics differ markedly among isotopes [35]. Thus, NRA offers possibilities for stable isotopic tracing investigations.

Analyzing the b product provides information about the A nuclei in the target, but b can be quite diverse, since there is a large variety of mechanisms that create different bs. One mechanism is a capture reaction, in which the target nucleus captures the incident beam to form a compound nucleus that subsequently decays through γ-emission, for example ^{7}Li$(p, \gamma)^8$Be. The second mechanism is when the compound nuclei breaks down in different fragments that can be particles or lighter nuclei, e. g. ^{7}Li$(p, \alpha)^4$He. The third mechanism takes place when the target nuclei is excited by absorbing part of the kinetic energy of the impinging particle which is inelastically scattered; the target nuclei de-excites emitting γ-rays, e.g. ^{7}Li$(p, p')^7$Li.

NRA with γ-ray detection is known as particle-induced γ-emission (PIGE). It is a technique employed extensively to detect light elements such as ^{7}Li [38] and ^{19}F [14]. For ^{6}Li analysis there is no usable γ-ray-emitting reaction [31]. Although PIGE seems to be a good alternative for light element quantifica-

tion [39], performing PIGE becomes difficult when the optimization of the sensitivity of different elements, by the use of different bombarding particles and energies, is required. According to Ref. [31], caution should be taken when PIGE is performed with ion energies close to the energies of sharp resonances since significant changes in the yield may caused by small changes in the ion energy.

A suitable method for selecting which nuclear process can be useful is to choose a reaction with high values of energy balance (Q) and cross-section (σ).

The reaction Q-value is the mass energy difference,

$$Q = (m_a + m_A)c^2 - (m_b + m_B)c^2, \tag{2}$$

that can be positive when energy is released, or negative when kinetic energy must be provided to the system $A(a,b)B$ [10]. The provided energy has to be higher than a threshold energy for this reaction. Reactions with high Q-values give products which are easier to detect as they have higher energies. Hence, the most useful nuclear reactions have large positive Q-values. Table 1 list Q-values of some reactions of interest for this work.

Table 1: Q-values in keV of the proton-induced (p,α) and deuteron-induced (d,α) α particle emission reactions with different nuclides.

Nuclide	(p,α)	(d,α)
^{6}Li	4021	22374
^{7}Li	17347	14230
^{10}B	1146	17811
^{11}B	8590	8031
^{16}O	-5218	3111
^{17}O	1193	9802
^{18}O	3980	4245
^{19}F	8115	10033

The cross-section σ is related to the reaction rate; if a reaction $A(a,b)B$ is taking place at certain rate, the event rate per nucleus exposed to the beam is proportional to the beam flux Φ [40], see Fig 2.5. The flux Φ is defined as the number of ions crossing a unit area per unit time. The proportional constant is called cross-section σ, which can be interpreted as a measure of the relative probability for a reaction to occur [41],

$$\sigma = \frac{\text{Reaction rate per nucleus}}{\text{incident flux}} \tag{3}$$

Reaction cross-sections are dependent on energy and angle of observation. Many cross-sections can be calculated based on nuclear physics models, however in IBA it is more common to use measured values published in the Ion Beam Analysis Nuclear Data Library [5]

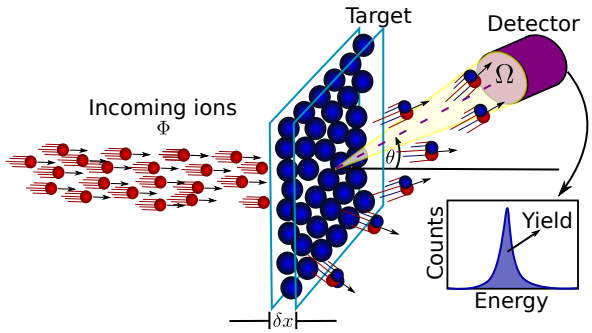

Figure 2.5: A charged particle flux irradiates a material with an atomic density N, number of atoms per unit volume. The emerging scattered particles are detected at θ. The total number of particle detected is known as yield Y.

2.3.2 *Reaction yields Y*

The yield Y of b products at a detection angle θ, when an ion beam a at energy E_a irradiates a target A, can be determined through the following relation [10],

$$Y = N\delta x \, Q \, \Omega \, \sigma(E_a), \tag{4}$$

where,

$$\begin{aligned} Y &= \text{ Yield, integrated peak counts} & N &= \text{ Atomic density} \\ Q &= \text{Incident ions} & \Omega &= \text{Detector solid angle} \\ \sigma(E_a) &= \text{Differential cross section at } E_a & \delta x &= \text{ Material thickness} \end{aligned}$$

This analysis is valid when the target is thin (hundreds of nanometers) and the cross section does not present abrupt variation in the vicinity of the energy E_a.

Use of standard samples

According to Eq. 4, the reaction yield provides information on the atomic density of a sample N, once the rest of variables are known. Unfortunately, these variables are not always easy to measure, so a sample with a well-known

concentration is utilized as a standard reference material (SRM) [31]. Thus, the total amounts of the measured nuclei for the unknown samples can be determined as,

$$N\delta x = (N\delta x)_{\text{Ref}} \frac{Y}{Y_{\text{Ref}}} \frac{Q_{\text{Ref}}}{Q} = \frac{Y}{Q} \left(\frac{N\delta x\, Q}{Y} \right)_{\text{Ref}} \tag{5}$$

For lithium and fluorine analysis performed in this work, a set of at least three reference materials were utilized to obtain better statistics of the factor $(N\delta x Q/Y)_{\text{Ref}}$. Minerals with a definite chemical composition and materials from the National Institute of Standards and Technology (NIST) were fit for use as standard reference materials. Typically, these samples are 5 μm in thickness, which is enough to fully stop the incoming ions passing thought the samples.

The changes of the ion beam energy within the samples, from an initial energy of E_a to zero, affects the reaction cross-section and in turns affects the reaction yield. Besides, the changes of ion energy makes the effective volume of material to be analyzed different per sample, since ions reach different depths in each sample before being fully stopped.

Ion beams can interact with atoms in a solid at different depths. Ions travel trough the sample undergoing collisions with atoms and electrons in the target. This makes ions lose energy and change their velocities. The path traveled between each collision and the energy loss per collision are random processes [10]. The energy loss per unit length in materials dE/dx is known as stopping power $S(E)$. A good estimation of $S(E)$ is considering atomic and electronic collision as independent mechanisms. Computer programs that treat ion-atom collisions with quantum mechanical approaches are good to calculate $S(E)$ values. Stopping and Ions Range in Matter SRIM is a well-known package that calculates $S(E)$ for different beam and material combinations [42].

Commonly, the reaction yields are corrected due to the stopping power $S(E)$. Through $S(E)$, the average length traveled by ions before stopping, called range (R), can be calculated. Thus, the reaction yield of particles emitted from a thick target becomes,

$$Y = N\, Q\, \Omega \int_0^R \sigma(E) dx = N\, Q\, \Omega \int_{E_a}^0 \frac{\sigma(E)}{S(E)} dE \tag{6}$$

The reaction cross-section is not constant across the thickness of a thick sample as it depends on the energy of the beam, which is slowing downs. A typical spectrum from particles coming from thick samples becomes the convolution of the concentration profile with the energy broadening of the incident ions

and the detected reaction particles [43]. Since the samples analyzed in this work were thick, only a depth defined by the range of the incoming ions was analyzed. Thus the reaction yield was calculated as,

$$Y \sim N\,Q\,\Omega\,\sigma(E_a)R \tag{7}$$

To ensure the samples are analyzed at the same depth, the volume was normalized using the one of the calculated range of the samples.

2.3.3 *Proton-induced and deuteron-induced α emission reactions*

Nuclear Reaction Analysis has been investigated by bombarding thin targets of well-known composition with different ions at well-defined energy. Nowadays in NRA, known reactions are observed and unknown targets bombarded [44]. In this work, well-known α-particles yielding reactions between protons and deuterons with lithium and fluorine were employed to evaluate lithium and fluorine concentrations in specimens with known and unknown elemental composition.

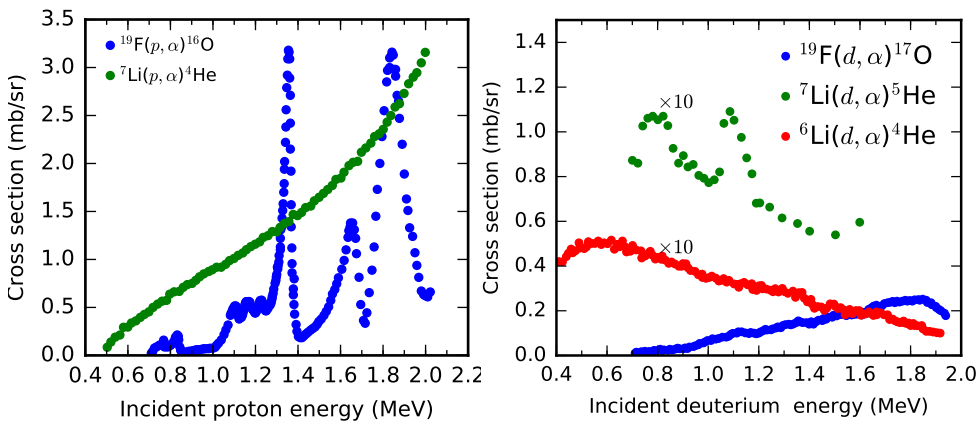

Figure 2.6: Cross-section as function of the incident proton (left) or deuteron (right) energies of ^{7}Li$(p,\alpha)^{4}$He [2], ^{19}F$(p,\alpha)^{16}$O [3], ^{6}Li$(d,\alpha)^{4}$He [2], ^{7}Li$(d,\alpha)^{5}$He [4] and ^{19}F$(d,\alpha)^{17}$O [2] reactions. Cross-section data were measured at $\theta = 150^{\circ}$ except for ^{7}Li$(d,\alpha)^{5}$He. Data taken from [5].

The NRA technique is grouped according to the type of ion that induces reactions and to the products emitted in the reactions. Thus, proton-induced and deuteron-induced α emission reactions are denoted as (p,α) and (d,α) respectively. The (p,α) reaction is the great interest for this work, since reactions

between protons with ^{7}Li and ^{19}F with α particles emission have high Q-values and present a reasonable high cross-section values as can be seen in see Table 1 and Fig 2.6. For ^{6}Li measurements it is more convenient to use the (d,α) reaction since its corresponding Q-value is much larger that the Q-value of the (p,α) reaction. see Table 1. In addition, there is much information reported regarding to the cross-section values of the (d,α) than the (p,α) reaction at the detection angles of interest. Chapters 4 and 5 describe the reactions between protons and deuterons with ^{7}Li, ^{6}Li and ^{19}F in more detail.

2.4 OTHER TECHNIQUES BESIDES IBA

Apart from IBA techniques, various methods have been utilized for elemental analysis in Earth sciences. Among these methods, Mass Spectrometry (MS), X-ray fluorescence (XRF) electron microprobe with energy-dispersive X-ray analysis (EDX) and neutron activation analysis (NAA) have being utilized [30]. All these techniques present advantages and disadvantages when multi-elemental analysis is performed. For instance, Mass spectrometry such as Thermal Ionization (TI), Inductively Coupled Plasma (ICP) and Sputtering (used in Secondary Ion Mass Spectrometry (SIMS)) have very high sensitivities [45]. However, samples have to suffer chemical preparation and also spectral interference can appear due to molecular or polyatomic formation produced by combination of two or more atomic ions coming from oxygen/nitrogen, surrounding air or from the solvent/sample [46]. On the other hand, XRF uses X-rays (primary) either from an X-ray tube or radioactive source to induce characteristic elemental x-rays (secondary or fluorescent) [47]. XRF and IBA have nearly the same relative sensitivity but not the same absolute sensitivity which might be important for some geological application as analysis of single grains of rare minerals [48]. In XRF corrections for matrix effect should be applied since primary and secondary radiation are attenuated in the specimen [29]. EDX and NAA also achieve equivalent concentrations as IBA techniques, nevertheless, IBA is superior in the minimum detectable concentration limits [49, 35].

The major drawback of IBA is that ion microprobe demands a million-volt particle accelerator and stronger focusing elements. In spite of this, IBA facilities are capable of carrying out RBS, PIXE, NRA, PIGE at the same time to a given sample.

3 LUND ION BEAM ANALYSIS FACILITY (LIBAF)

The use of IBA techniques requires sophisticated equipment such as accelerators, vacuum chambers, and a number of radiation detection systems. These instruments can be found at the Lund Ion Beam Analysis Facility (LIBAF), where the work presented in this thesis was performed.

Different types of charged particles with defined energies are obtained from the accelerator, which steer the charged particles towards a target. The reaction products from the interactions between the incident beam and the target atoms can be registered by the use of radiation detectors combined with a data acquisition system. Depending on the type of the emission products (charged particles or electromagnetic radiation), various detector systems can be used.

This chapter describes the basic concepts around an electrostatic accelerator of the Van de Graaff type and α-particle and X-ray detectors connected to a multi-parameter data acquisition and control system.

3.1 ELECTROSTATIC ACCELERATOR

The LIBAF has a 3 MV single-ended Pelletron accelerator based on a Van de Graaff generator. This accelerator, designed by the National Electrostatic Corporation, is capable of delivering three species of ions, H^+, D^+, and He^+, with achievable energies up to $E = q \cdot V$, where q is the ion charge and V is the electric potential. Further capabilities and features of the LIBAF are described in Refs. [50, 7, 12].

A schematic diagram of the accelerator is illustrated in Fig. 3.1. The accelerator consists of a large hollow metal semi-sphere and a Pelletron charging chain. The hollow metal is an isolated terminal which can be charged up by means of charge sprayed onto the moving chain. The Pelletron chain is made of metal pellets coupled by insulating nylon links [51]. Charge is induced on the chain through inductor electrodes connected to external 50 kV power supplies. The accelerator system is placed in a pressure tank filled with SF_6 that inhibits breakdown and sparking.

The heart of the accelerator is a radio frequency ion source, that is situated inside of the hollow conducting shell. The source produces 3 keV to 5 keV positive ions of hydrogen and helium [52]. An extractor, Einzel lens and

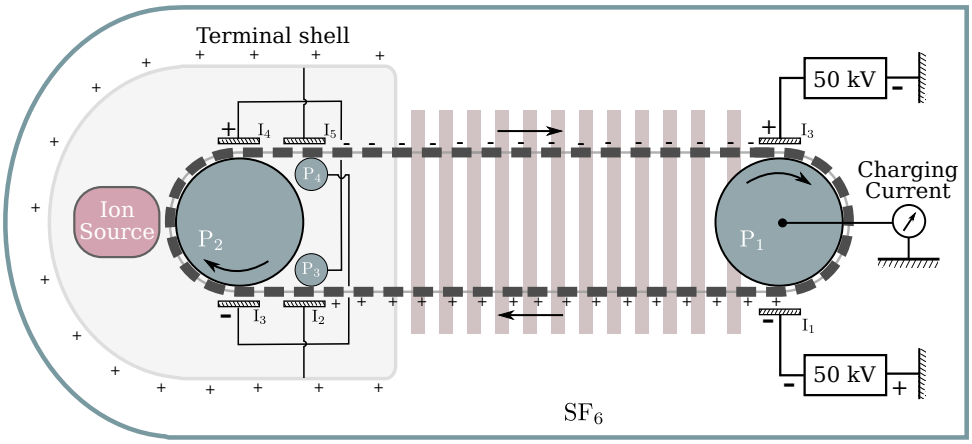

Figure 3.1: Schematic diagram of a Pelletron accelerator based on a Van de Graaff generator. This drawing is inspired by the sketches of Ref. [6]

velocity selector are used to select the desired beam according to the charge state and mass of the ions.

3.2 BEAM TRANSPORT AND FOCUSING

Ions must be transported from the accelerator to an experimental chamber where a small sample (area about $500\mu m \times 500\mu m$) is located to be irradiated. Thus, outside of the accelerator, the ions are transported along a beam line, where a magnetic quadrupole lenses, aperture slits, beam stops and beam viewers are installed to focus, control and optimize the size and the current of the beam. Fig. 3.2 shows a schematic illustration of the Lund Ion Beam Analysis Facility, which consists of an accelerator, experimental chambers and two beam lines with a focusing system.

The great advantage of using a focused beam is to obtain details of the 2D-distribution of elements over a specimen [52]. To confine the ion beam to a small spot, the beam is collimated with two pairs of slits set at $10\mu m$ each. One of the pairs slits was located near the beginning of the beam line and the other near to a set of magnetic quadrupole lenses. The slits allow the final spot size of the beam to be defined, then the beam is focused by the quadrupole lenses. These lenses are comprised of three quadrupole of alternating polarity.

The elemental distribution of a sample can be obtained with a scanning system, which sweeps the beam relative to a static target. At LIBAF, the

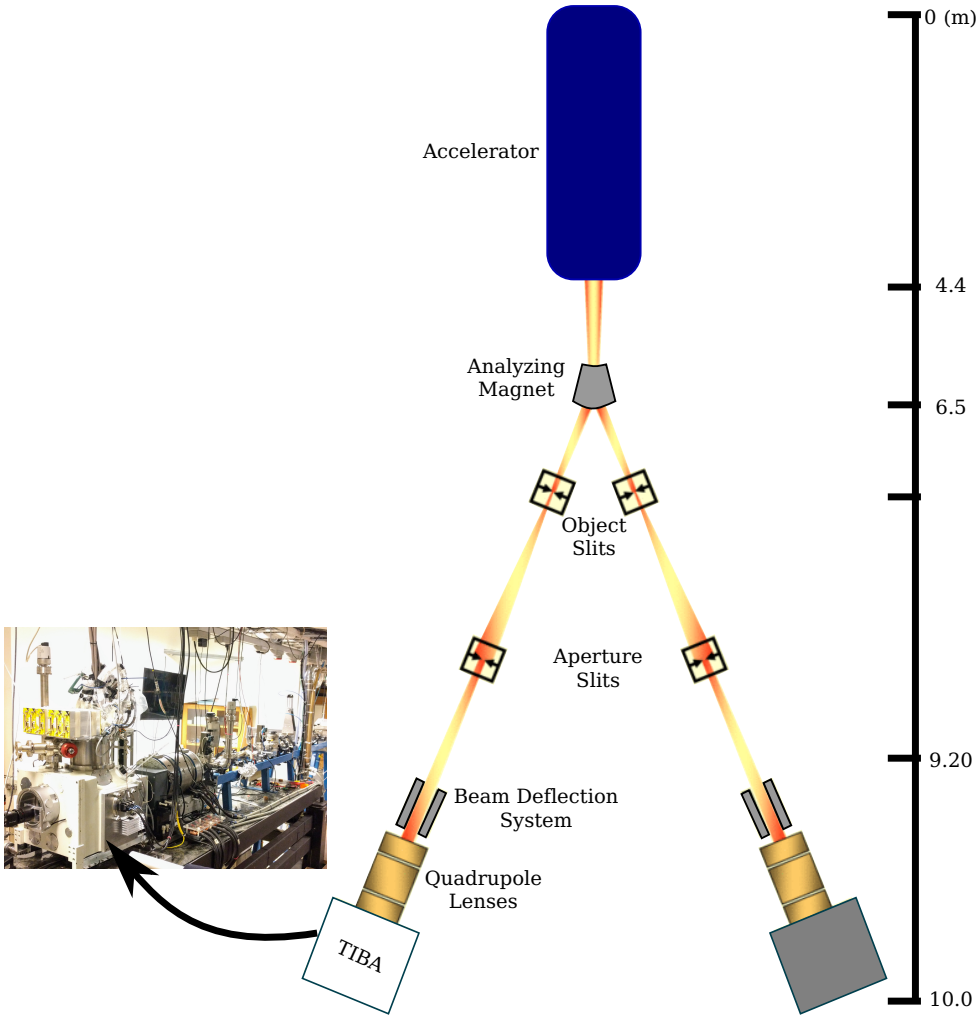

Figure 3.2: A schematic illustration of the Lund Ion Beam Analysis Facility. It has a 3 MV single-ended accelerator, two beam lines, two chambers: sub-micro and a Total IBA (TIBA). The inset shows a picture of an extension of the left beam line, which is connected to the new total IBA chamber. The LIBAF diagram has been modified from Ref. [7]

scanning system has the possibility to be programmed to swipe the beam across regular or irregular shapes on a target.

3.3 BEAM CHARGE MEASUREMENTS

Two experimental setups, a manual and a new digitally controlled system, were employed for charge measurements. The new system is an upgrade that was developed recently and has been used for the fluorine analysis in Paper IV. A detailed description of the system is founf in Paper III.

The beam charge, Q, is proportional to the number of ions that impinged on a sample during a time interval and is related to the yield of the reaction products, see Eq.4. It is therefore of the utmost importance to determine Q accurately. To determine Q, a pair of parallel metal plates connected to a high voltage pulse generator module (PVM-4210) deflects the beam into a pre-sample Faraday cup [53] where a charge integrator measures the charge during a certain period of time. This method gives charge measurements independent of the conductivity and structure of the sample. For lithium and fluorine analysis, the beam is deflected for one second every ten seconds. The charge collected over the one second deflection time is assumed to be the constant value of the current (I) for the next ten seconds. While the sample is being scanned with the beam, the analyzing time (t_A) for each scan point is registered and the charge collected per scan point can be estimated as $I \cdot t_A$. The charge measurement precision is around 3% in this work.

A manual system for setting up the deflection voltage to the Faraday cup has been in place for many years at the LIBAF. The voltage is operated through a pair of potentiometers on the high voltage pulse generator module. The optimal deflection voltage is the one which steers the beam directly into the center of the Faraday cup. Under this condition the measured current will be observed to maintain a stable maxima for small voltage variations and should therefore remain stable for small variations in beam alignment due to low-level beam instability. Failure to meet this condition means introducing large uncertainty into the current measurement which in turn results. in an incorrect interpretation of the experimental results. This optimal deflection voltage is unique to the energy and mass of the beam particles, and also to the alignment of the beam between the metal plates.

The results for Paper I and Paper II were obtained using protons with energies around two main energy values: 800 keV and 2500 keV. The rather small variations around 800 keV or around 2500 keV did not require significant changes to the deflection voltage. For experiments where a beam energy scan had to be performed, the deflecting voltage had to be adjusted multiple times. In order to reduce the risk of misdirecting the beam into the Faraday cup, a new digitally controlled deflection set-up was installed.

The new digital set-up to control the beam deflection is comprised by an electronic unit that automatically scans the beam deflection voltage over a given range. This new control system was designed specially for the TIBA chamber but it can be used for other beam lines at the LIBAF. For more details of its configuration, operation, and its Graphical User Interface (GUI), the reader is referred to Paper III. The new system has at its core a Teensy 3.2 microcontroller [54] to set and read in the voltage on the deflection plates along with the charge measured in the pre-sample Faraday cup and in a sample located inside the TIBA chamber. An example result is shown in Fig 3.3. The plot shows the ratio between the charge in the Faraday Cup and the charge on the sample as a function of the deflection voltage for a proton beam energy of 2500 keV. A ratio of one is desired for a proper beam deflection. The approximately constant value obtained in the region between 950 V-1300 V shows a beam correctly impinging into the Faraday cup. A value of ∼1150 V was selected as the optimal voltage to be used during the experiment at this beam energy.

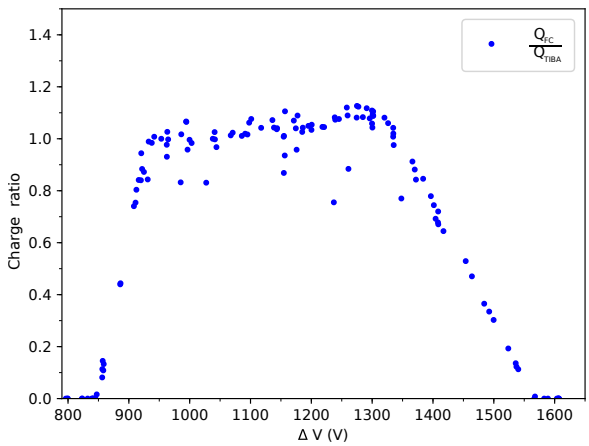

Figure 3.3: Ratio between the beam charge measured in the pre-sample Faraday cup, Q_{FC}, and in a copper plate inside the TIBA chamber, Q_{Tiba}, as a function of the deflection voltage between the deflector plates, ΔV, using the new control system for a 2500 keV proton beam. From this plot, a value of ∼1150 V would be an optimal voltage to use.

3.4 DETECTORS

3.4.1 *Charged-particle detection*

Charged-particle detection was carried out employing a semiconductor particle detector, a CD-type 310 μm thick double sided silicon strip detector (*DSSSD*) [9] with a 90 V depletion voltage. Its outer active diameter is 85.4 mm and its inner active diameter is 32 mm. Assuming a sample located at 26 mm from the detector, the covered active solid angle is 2 sr [55], see Fig.3.4.

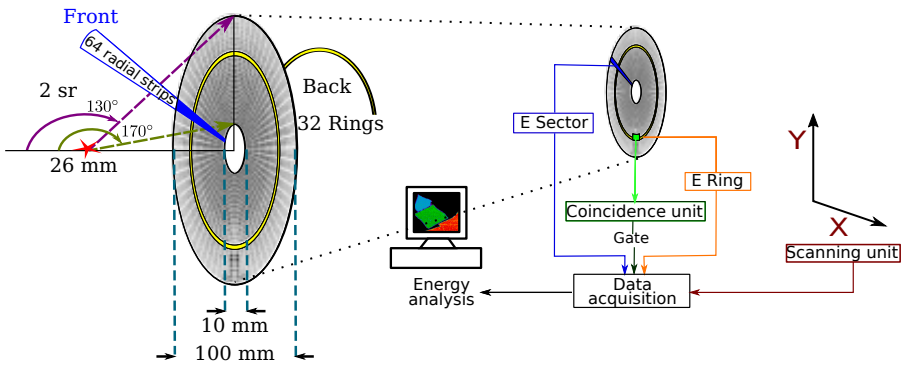

Figure 3.4: Double sided silicon strip detector (*DSSSD*) with 64 radial strips (sectors) and 32 concentric circle strips (rings). Assuming a sample located at 26 mm the covered active solid angle is 2 sr. On the right, a schematic diagram of how a signal is processed at LIBAF is shown, see Sec. 3.5

The *DSSSD* name comes from being doubly doped on each side. Boron was implanted on one side to obtain p-type regions and the other side, n-type donors were implanted to acquire n^+-regions. Both sides of the detector are covered with metal strips to create electrodes through which signals can be extracted. The p-type side presents 64 radial strips (sectors) from the center to the edge of the detector, while the n^+-region side presents 32 concentric circle strips (rings). Typically, the sectors side is facing the radiation source, for that reason it is named the front side while the rings side is the back side. The metal sectors side is perpendicular to the metal rings side, which creates $64 \times 32 = 2048$ detector elements (cells or pixels). An electric field is created between the electrodes of each pixel, see Fig.3.4. This electric field determines an active volume or zone [9]. Each detector cell has characteristics similar to a standard surface barrier detector (SBD).

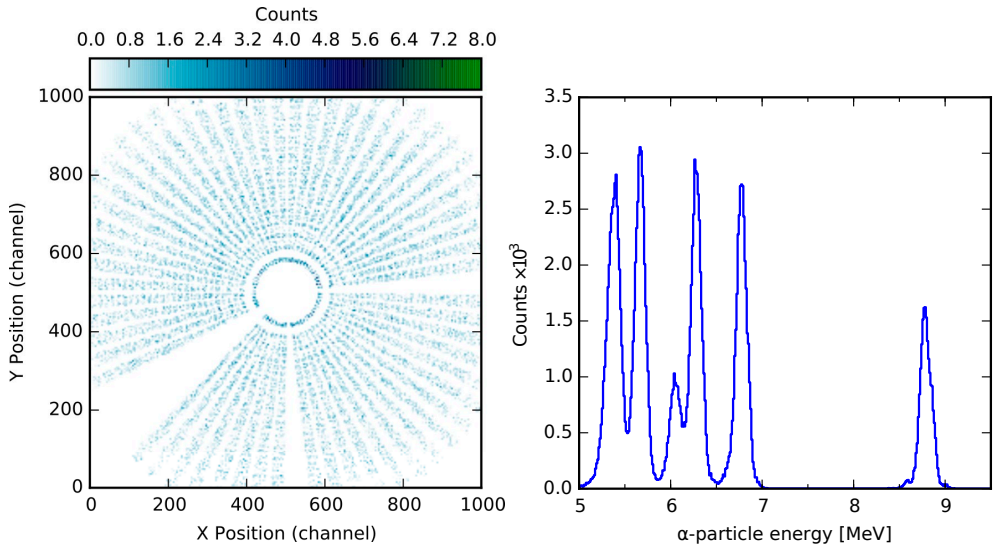

Figure 3.5: α particles from a ^{228}Th source detected by the DSSSD. Left: number and position of α particles detected in each pixel. Right: Calibrated energy spectrum. There are four radial strips and one ring electrode not working.

When a charged particle hits the detector, electrons and holes are generated. Both types of charge carriers are subsequently swept by the electric field to the p-electrode and n^+-electrode in the active volume [56]. The charge collected by each detector element (sector or ring) on each of the two detector faces is proportional to the deposited energy of the impinging charged particle.

The sectors and rings of the DSSSD were calibrated in energy using a ^{228}Th α source. This source transmutes into ^{208}Pb through a chain of α decays. In this process, α particles with energies ranging from 5.4 MeV to 8.78 MeV are emitted [57]. The typical energy resolution of a sector or ring is 0.5 % (44 keV FWHM at 8.78 MeV) [9]. The calibration spectrum as well as the counts per pixel of the detector are displayed in the Fig. 3.5.

There is a tiny layer of the detector which is not sensitive to the passing of radiation, known as dead layer; it is composed of a mixture of silicon, silicon oxides and the metal strips with a thickness of $\sim 2\mu$m [9]. If the dead layer is simplified as SiO_2, for an 8-MeV α particle the stopping power is 115 keV/μm with a total range of 45 μm [42]. The energy lost by the α particle when it passes the dead layer is about 250-300 keV.

3.4.2 *X-rays detection*

Characteristic X-rays induced in the interaction of ions with target atoms were detected with a 150 mm^2 KETEK VITUS CUBE Silicon Drift Detector (SDD). This detector has an energy resolution of $\leq$ 136 eV at 5.9 keV [8]. A typical spectrum of a SDD is exhibited in Fig 2.4.

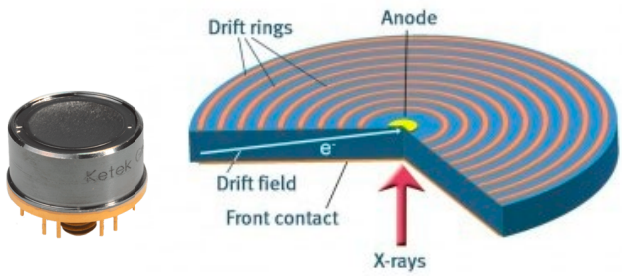

Figure 3.6: 150 mm^2 KETEK VITUS CUBE Silicon Drift Detectors (SDD). Figure adapted from Ref. [8].

Fig 3.6 shows schematically the working principle of a SDD. This detector is a high-resistivity silicon disc which is fully depleted when a negative bias voltage is applied to both sides [58]. A potential gradient between the drift rings is created. Thus, when electrons formed by the ionizing radiation within the SDD, they are directed parallel to the surface towards a small charge collecting anode in the center [59].

3.5 ELECTRONICS AND DATA ACQUISITION

Current pulses coming out from the DSSSD are small signals that can be affected by noise in long cables. To process such signals, they must be amplified by a charge sensitive pre-amplifier [41], which must be located as close as possible to the detector. The DSSSD has 64+32=96 electronics channels. The current pulses are pre-amplified by 6 mesytec MPR-16 modules (16 ch. each) [60]. Once the energy signals are preamplified, they are sent to MSCF-16-F shaper modules where the signals are shaped into Gaussians forms and amplified again. The energy signal from the SDD comes preamplified already and it is sent directly to a MSCF-16-F amplifier module.

The analogue-to digital conversion of the signals is carried out by V785N and (3x) V785 ADCs from CAEN readout at a Versa Module Europa (VME) crate.

For details about the scanning system, and charge measurements controlled by the DAQ at the LIBAF, the reader is referred to Ref. [61].

The energy signals coming from the front side and the back side of the DSSSD are connected to a coincidence unit. A schematic diagram of the modules and electronic connections are shown in Fig. 3.4.

There are some issues such as pile-up effect and DAQ dead time when signals are digitized and processed. The pile-up effect is an event which contains the overlap of more than one energy signal. The energy of such an event is the total or partial energy sum of the incoming signals. The dead time of the system is the time while the electronics modules and readout system are busy processing a signal. The devices need some time to be ready for the next event. The data acquisition system has a characteristic response time that depends on the detector, preamplifier, shaper, ADC, and readout chain.

A typical semiconductor detector has an average rise time of $\sim$30 ns. The amplifier can shape an incoming signal of about 500-4000 ns, which is adjustable by the user. Finally, a signal is sent to analogue-to-digital converters (ADC) which process the signal on 6-10 μs per channel. Within this time, the ADC is busy and it can not process any new incoming signal. While the ADC is busy, the time is measured and it corresponds to the dead time of the system [62].

To reduce the occurrence of pile-up it is possible to decrease the count rate of detection system by reducing the beam current, shortening the shaping time of the signal at the expense of energy resolution. Thanks to the high granularity of the DSSSD there is no need to reduce the beam current nor to modify the shaping time of the signals.

Fig. 3.7 shows an α-particle spectra taken with an ordinary annular surface barrier detector (SBD) and with the sum of the front side of the DSSSD detector [9]. Approximately, the same solid angle is covered by both detectors. The reaction under study was ^{23}Na(p, α)^{20}Ne, which was induced with protons at 620 keV. A marked pile-up effect is presented in the SBD spectrum, whereas the DSSSD spectrum exhibits well-defined peaks.

3.6 SAMPLES AND SCANNING AREAS

IBA techniques require minimal sample preparation; generally speaking, the samples must be prepared for examination at high vacuum ($\sim 10^{-6}$ mbar) and for irradiation with a ion beams. In geological applications, the samples are mineral inserted in epoxy that are subsequently polished to obtain a flat sample surface facing the ion beam. The mineral are commonly embedded together as seen in Fig. 3.8.

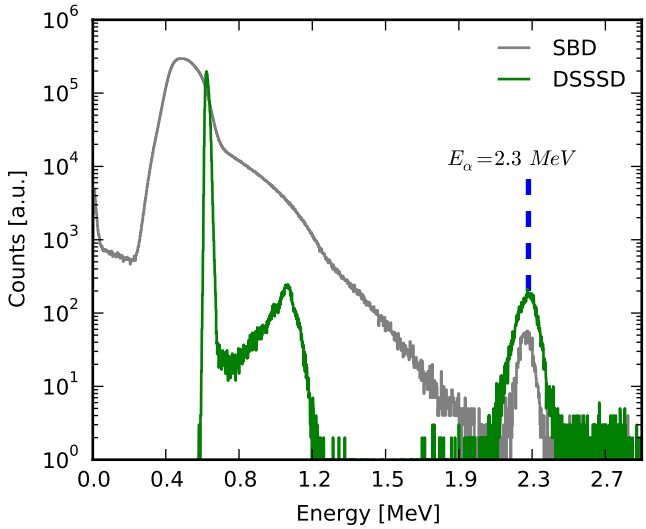

Figure 3.7: Energy spectrum of α particles from the ^{23}Na(p,α)^{20}Ne reaction at $E_p = 620$ keV. This reaction was performed at two different beam currents, the gray spectrum was taken with a SBD using a 200 pA beam current and the green spectrum was taken with a DSSSD using a 2 nA beam current [9].

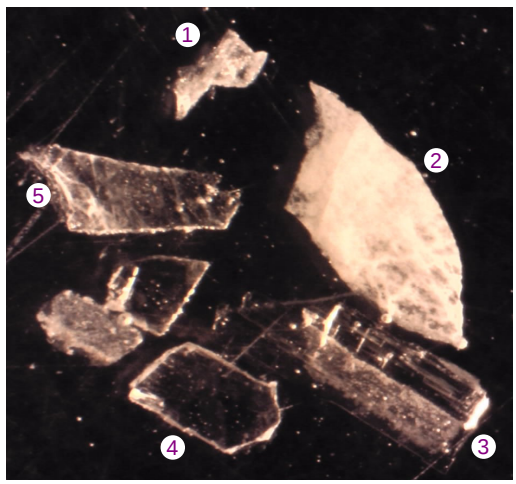

Figure 3.8: Typical embedded sample, it contains Li-bearing minerals, 1:Lithiophosphate Li_3PO_4, 2: Amblygonite $LiAl(PO_4)F$, 3: Spodumene $LiAlSi_2O_6$, 4: Petalite $LiAl(Si_4O_{10})$, 5:Eucryptite $LiAlSiO_4$. This photo is a courtesy of The Swedish Museum of Natural History.

Two types of samples have been used in the experiments, reference standards and geological samples. The standard reference materials (SRMs): 610 [1] and 612 [1] manufactured by The National Institute of Standards an Technology (NIST) have been chosen for their well-known composition, which is of great importance in determining the relation between elemental compositions and yields. The geological samples, tourmaline crystals, Li-bearing and F-bearing minerals, used were provided by The Swedish Museum of Natural History, Stockholm, Sweden. It should be noted that the composition was previously known only for some of the geological samples.

Since a typical sample consists of a set of embedded crystals, the first step of analysis is to select a scanning area of a crystal of interest. The crystal location can be set optically or using backscattered protons. Optical location provides a rough idea about the sample position, whereas imaging reconstruction through backscattered protons enables the selection of an area inside of the crystal of interest.

Geological materials are inhomogeneous structure consists of heterogeneous assemblages of minerals containing diverse elements in a great variety of chemical states. Commonly within geological material there is a matrix of major elements, such as O, Na, Mg, Si, Al, S, K and Ca, combined with a large number of minor and trace elements [29] The concentration of major and minor trace elements is determined throughout creation of the minerals by factors such as temperature conditions and chemical environment. Subsequently, the concentration is altered by processes of diffusion, leaching and dissolution. Thus, the investigation of trace element concentration in minerals gives clues about the genesis and physico-chemical history of the geological samples.

4

DETERMINING LITHIUM CONTENT

Lithium is a tracer element that enables the investigation of geological processes such as magmatic differentiation [28], seawater-basalt interaction, and crust-mantle recycling [63]. Lithium is of great interest in medicine, cosmology, materials science, among others areas. Lithium is also very popular due to its use in lithium-ion batteries, see Nobel prize in chemistry, 2019. Currently, the subject of comprehensively understanding the lithium transport in the batteries is being approached by the investigations of the depth distribution of lithium in the anode and the cathode of lithium ion batteries using IBA techniques [64, 65].

Lithium, the third element in the periodic table, has two stable isotopes ^{7}Li and ^{6}Li, of which atomic abundances are approximately of 92.41% and 7.59 % respectively [66]. The system of three protons plus three or four neutrons is detectable through its interactions with accelerated protons, deuterons, and α particles. However, the detection of lithium is not easy since it is highly reactive and is therefore not found in its elemental form in nature. One of the challenges of lithium isotope detection is filtering out reaction products from other elements that may be present in the samples. Precise measurements of low-mass isotope fractionation is difficult [66], but NRA provides a method for lithium determination without that difficulty.

This work consisted in establishing a technique for lithium measurements in materials based on NRA. Yield and mapping possibilities of lithium and heavier elements in geological and standard reference samples were demonstrated by using PIXE simultaneously with NRA. All this work is condensed in two articles. The aim was to address the challenge of measuring ^{7}Li at very low concentrations. Measurements of ^{6}Li have also been attempted (work in progress) and some preliminary results are found in this chapter. In Paper I, a set of experiments was conducted in order to find an appropriate proton beam energy, which can induce the ^{7}Li(p,α)^{4}He reaction in lithium-bearing materials. Paper II presents the validations of the methods found in Paper I using samples with various lithium concentration. In addition, PIXE was used as a complementary technique to evaluate the possibility of detecting elements with $Z > 20$.

As part of an exploratory study of the possibility to quantify ^{6}Li and ^{7}Li using deuteron-induced reactions at LIBAF, the ^{6}Li(d,α)^{4}He and ^{7}Li(d,α)^{5}He

reaction was investigated using different beam energies. Interferences from other reactions were also explored.

4.1 PROTON-INDUCED REACTION ON LI-BEARING MATERIALS

When protons initiate reactions in a target nuclei of ^{7}Li, different reaction products are created. Fig. 4.1 displays the cross section (σ) for a variety of possible products from different reactions with ^{7}Li. Within these reactions resonance scattering (p, p), γ emission (p, γ), neutron emission (p, n) and α particle emission (p, α) reactions may take place. In the case of the (p, α) reaction, its cross section varies smoothly as a function of the incident proton energy E_p, in the energy range shown. For the other cases, marked resonances arise.

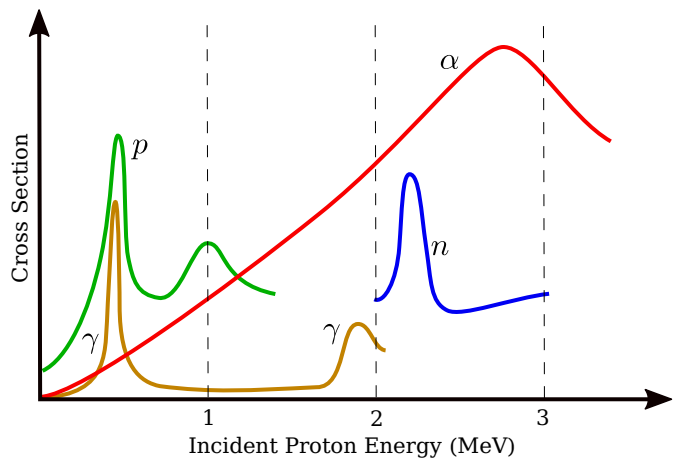

Figure 4.1: Cross section as a function of the proton energy of the possible products from the reaction between ^{7}Li and energetic protons. Figure based on Ref. [10]. Resonance scattering (p, p), proton-induced γ emission (p, γ), proton-induced neutron emission (p, n) and proton-induced α-particle emission (p, α).

The reasonably favorable cross-section of (p, α) relative to the other cross-sections makes the ^{7}Li(p, α)^{4}He reaction a good candidate to quantify ^{7}Li. This reaction also has a high Q-value of 17.3 MeV and no major interference from other reactions [31]. Thus, the detection of α particles from the ^{7}Li(p, α)^{4}He reaction was selected as the method to determine the amount of ^{7}Li in geological samples.

Quantification of ^{7}Li using the ^{7}Li(p, α)^{4}He reaction

When the ^{7}Li(p, α)^{4}He reaction occurs, it implies that per each ^{7}Li atom an α particle and an ^{4}He atom are emitted. Thus, this reaction enables the ^{7}Li quantification by collecting the ejected α particles. When these particles are detected, they will form a distribution around a certain E_α energy. Therefore, the intensity of the distribution (α-particle yield) can be converted to elemental concentrations of ^{7}Li.

The E_α energy can be deduced by applying the conservation laws of energy and momentum. Fig 4.3 illustrates the nuclear reaction process and shows the reaction parameters, as the values of the E_α and $E_{^4\mathrm{He}}$ energies, when a proton at 0.8 MeV hits a ^{7}Li target. For this case, the E_α energy is 7.7 MeV, at which, a distribution is formed in the spectrum also displayed in Fig 4.2.

A proton beam can induce the ^{7}Li(p, α)^{4}He reaction as well as ^{19}F(p, α)^{16}O, if the bombarded sample also contains fluorine. α particles from both reactions can have similar energies leading to interference for ^{7}Li analysis. However, It is possible to avoid this interference by selecting incident proton energies appropriately.

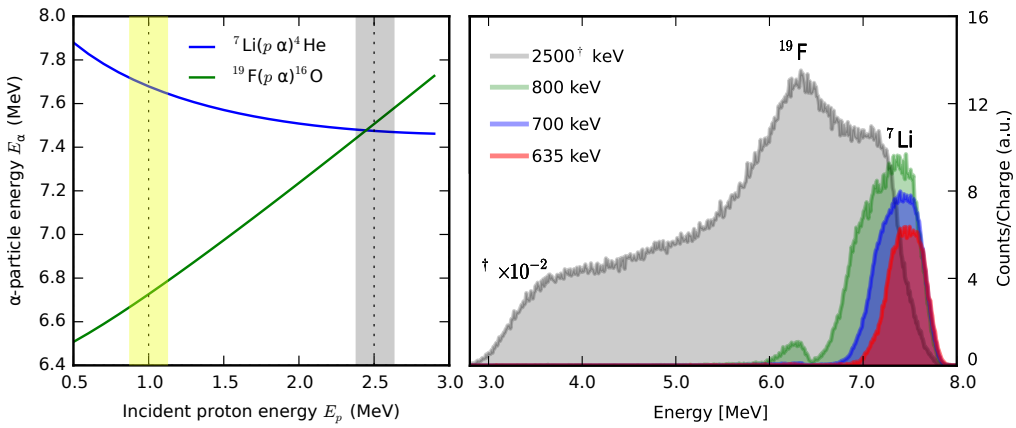

Figure 4.2: Left: α-particle energies (E_α) as a function of the incident proton energy (E_p), values from kinematic calculations using a dispersion angle $\theta = 170°$. Right: experimental spectra of α particle coming from a LiF sample bombarded with various proton energies. This result comes from Paper I [11].

By the use of different incident proton energies, α particles from the ^{7}Li(p,α)^{4}He reaction are ejected at different energies. The energy dependence of the α particles on the incident proton energy E_p can be seen in Fig 4.2. The plots show results from kinematic equations calculated with a detection angle equal to

170°. The energies of the α particles produced by the ^{19}F presence (green line) and the ^{7}Li (blue line) overlap at around E_p ~2.5 MeV. Thus, simultaneous detection of ^{7}Li and ^{19}F is possible when the E_p energy takes values away from the vicinity of 2.5 MeV. Fig 4.2 also shows experimental energy spectra of α particles from a LiF crystal, which was irradiated with a proton beam at 2500 keV, 800 keV, 700 keV and 635 keV. An well-separated fluorine peak can be seen when using a proton energy of 800 keV.

Other reactions such as ^{18}O(p,α_0)^{15}N, ^{11}B(p,α_0)^{8}Be, ^{11}B(p,α_1)^{8}Be* and ^{15}O(p,α)^{12}C can take place under the same conditions as the ^{7}Li(p, α)^{4}He reaction. However, the energy distribution of the detected α particles can be broad and cross each other. For that reason, multi-elemental analysis of light elements can be carried out by simultaneously selecting an appropriate energy window for the resulting α particles in combination with an adequate energy of the proton beam. Fig 4.3 shows energy spectra of the emerging α particles from a standard reference sample (NIST 610 [1]) irradiated with a proton beam at 800 keV. Lithium, boron, oxygen and fluorine can be identified in the spectrum.

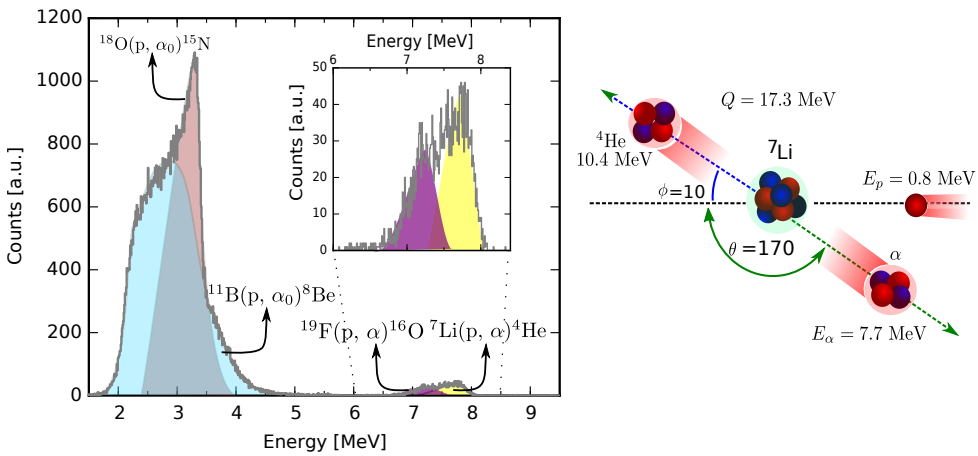

Figure 4.3: Left: Energy spectrum of α particles produced by bombarding a standard reference sample (NIST 610 [1]) with a proton beam at 800 keV; the inset is a zoom in of the spectrum that shows lithium and fluorine signals. Right: the ^{7}Li(p, α)^{4}He reaction which took place in this experiment is schematically represented.

Lithium measurements were performed in two stages. In the first stage, the dependence of the lithium yield and the background contribution as a function of the proton energy was investigated. In the second stage, the lithium technique developed in the first stage was validated by the analysis of minerals with various amount of lithium. In both parts, common procedures such as

sample preparation and selecting scanning areas of interest in the samples were carried out. The next section gives a brief explanation of the experimental steps followed to address the challenge of measuring ^{7}Li using IBA techniques.

^{7}Li yield and background contribution as functions of the proton beam energy

In this part, two questions are answered: What proton beam energy is appropriate to obtain a background-free α-particle spectrum? and What is the relation between ^{7}Li yield and ^{7}Li content? Paper I describes the process for addressing these questions. The answer to the first question came from a set of experiments that consisted in measuring α particles produced by scanning a LiF crystal at 635 keV, 700 keV, 800 keV and 2500 keV proton beam energies, over 10 minutes, see Fig. 4.2. The most appropriate proton beam energy with clear separate peaks was found to be 800 keV, see Paper I [11] for the full discussion. This energy was used to irradiate the NIST 610, NIST 612 and the tourmaline standard samples. Since these samples have well-known lithium content, it was related to the α-particle yield in each sample. All the required experiments in this part were carried out in the experimental chamber of the sub-microbeam line shown in Fig. 4.4.

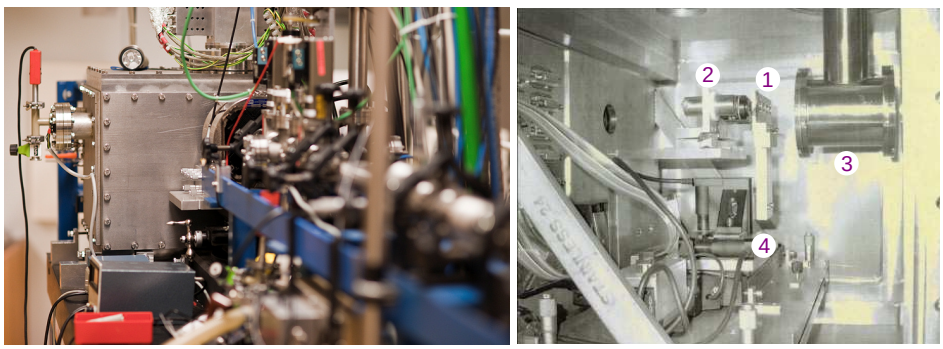

Figure 4.4: Right: Experimental chamber used for high-resolution nuclear microprobe applications. Left: Inside view of the chamber; photo taken from Ref. [12]. The main components located inside are: 1: Sample holder, 2: Microscope, 3: Place for the DSSSD. 4: XYZ-movable stage.

^{7}Li technique validation

The lithium analysis technique developed in the first part of this work was validated using the new total IBA chamber installed recently at LIBAF, see Fig 4.5. In addition, a multi-elemental analysis was performed. Paper II

presents this research. The validation of the lithium technique consisted in measuring the lithium content in Li-bearing samples whose concentrations range from 2% to 18%. α particles produced from the induced reactions in these samples were detected. Fig. 4.6 shows the α-particle spectra measured. In each spectrum, two types of peaks are exhibited, one around 3 MeV, that corresponds to oxygen, and other around 7 MeV, that corresponds to lithium. The intensity (total counts) of the lithium peak is related to the lithium content in the samples, the sample with the highest lithium concentration has a peak with the highest intensity.

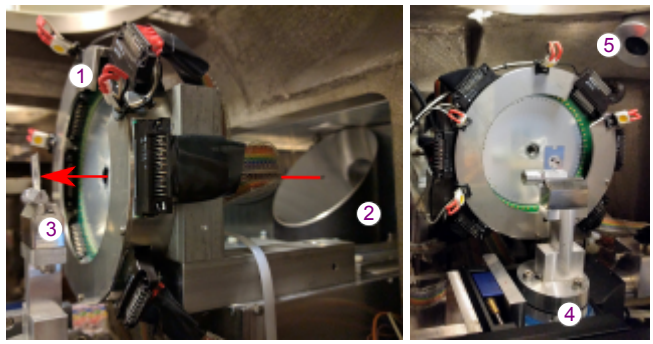

Figure 4.5: Inside view of the new total IBA chamber. Left: This picture shows the set-up employed for NRA experiments. Right: This view shows how a 50 mm^2 silicon drift detector was placed to detect X-rays for PIXE. The chamber is equipped with the following components: 1: Annular detector DSSSD, 2: Mirror to focus the beam, 3: Sample holder, 4: XYZ-movable stage (scanning unit), 5: X-ray detector.

Lithium measurements limits were also evaluated using a Suprasil quartz (Li-free crystal). This sample was scanned with a proton beam at 800 keV for three hours. The α particles detected during this time came from the $^{18}O(p,\alpha_0)^{15}N$ reaction. An energy spectrum of the α particles is shown in Fig. 4.7. If ^7Li had been present in the sample, the spectrum would show entries in the 7-8 MeV energy range (see green area in Fig. 4.7).

Regarding the multi-elemental analysis, boron and heavier elements such as calcium and iron were detected at the same time using a suitable proton beam energy which was 850 keV. 2D lithium, boron, calcium and iron distribution maps of a tourmaline standard are shown in Fig. 4.8. Lithium and boron maps are results from NRA while maps of calcium and iron were obtained using PIXE. The 2D maps are obtained selecting a specific energy range of the α particles and X-rays. For example, 2D lithium distribution map shows the α-particle counts detected by the DSSSD for α particles with energies within

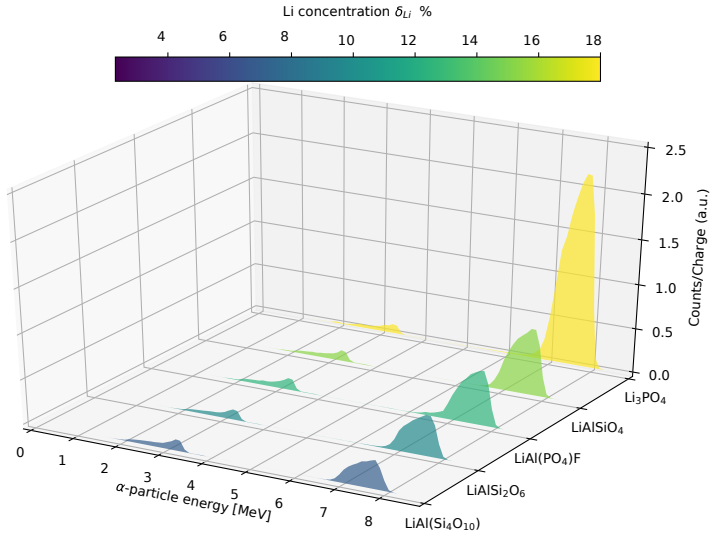

Figure 4.6: Normalized energy spectra of the α particles from the ^{7}Li(p, α)^{4}He reaction induced in the Li-bearing samples shown in Fig. 3.8. The color bar indicates the level of lithium concentration in the samples.

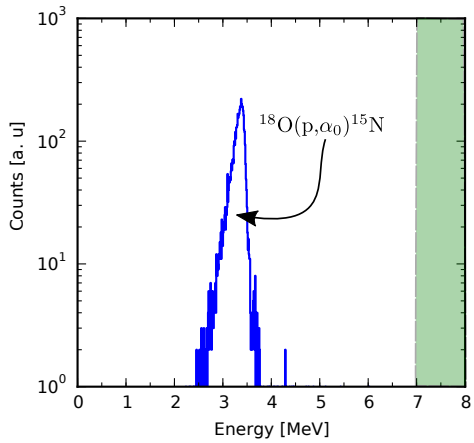

Figure 4.7: Spectrum of the α particles from a Suprasil quartz (Li-free crystal). This sample was bombarded with a proton beam at 800 keV for three hours. The green area covers the 7-8 MeV energy range where there are not registered events. This indicates ^{7}Li is not present in the sample.

7-8 MeV range. To extract boron contributions, α-particle energies were selected within the energy windows 3.3-4.3 MeV, according to the study conducted in Ref [21].

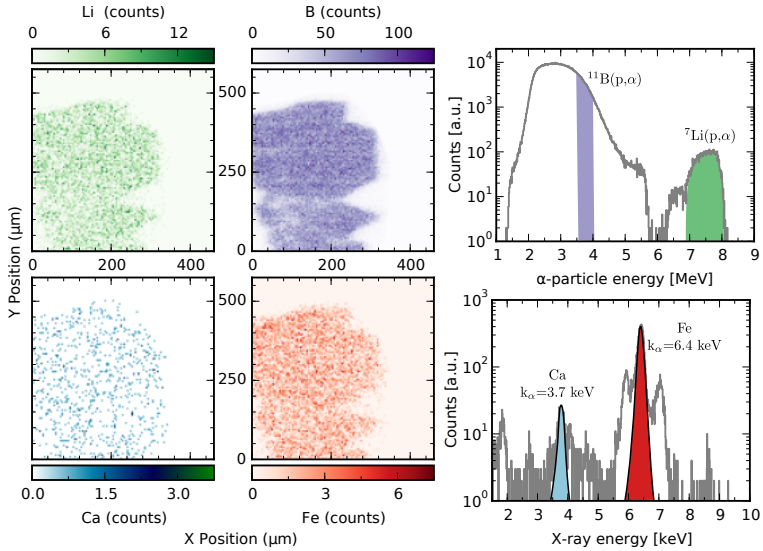

Figure 4.8: 2D lithium, boron, calcium and iron distribution maps of a tourmaline standard sample. The spectra are formed with α particles and X-rays emitted when a tourmaline was bombarded with a proton beam at 850 keV for 10 minutes.

The relation between lithium concentration and boron in tourmaline samples was also studied. The purpose of this study was to examine a possible pattern of lithium presence in the tourmalines where boron concentration is approximately constant. The results of this study are presented in Paper II.

4.2 DEUTERON-INDUCED REACTION ON LI-BEARING MATERIALS

Most of the light elements can interact with deuterons through exothermic reactions. In the case of lithium isotopes, deuteron-induced α-particle emissions present high $\mathcal{Q}$-values, as can be seen in Table 1. Some results of a preliminary study of deuteron-induced reactions on Li-bearing materials are presented below.

The ^{6}Li(d, α)^{4}He reaction has a $\mathcal{Q}$-value of 22 MeV, a quantity that far exceeds the $\mathcal{Q}$-value of the (p, α) reaction, which in turn is a very good reaction to quantify ^{7}Li, see Table 1. The reactions between ^{6}Li and deuterons lead to the production of protons from the $^{6}\mathrm{Li}(d, p_{[0,1]})^{7}\mathrm{Li}$ reaction that can be used for ^{6}Li analysis. For this reason, deuteron-induced reactions are superior to proton-induced reactions to detect ^{6}Li.

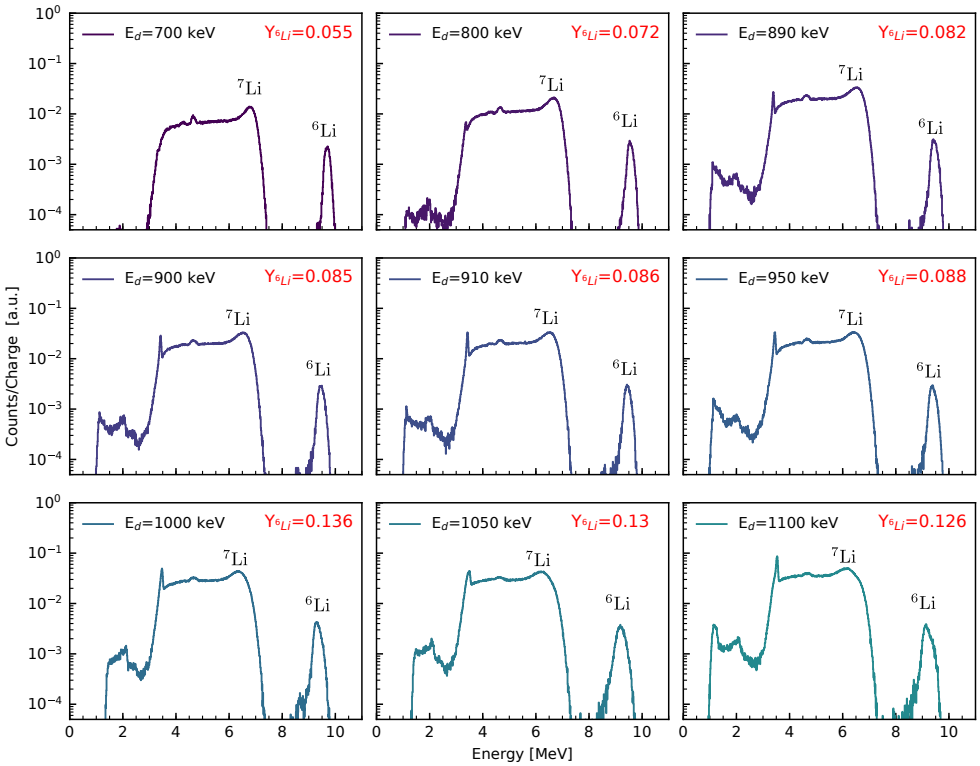

Figure 4.9: Energy spectra from a Li_3PO_4 mineral for different incident deuteron energies. The ^{7}Li and ^{6}Li content is represented by the peaks at 6.5 MeV and 9.2 MeV respectively. The peak that can be discerned at 4.5 MeV corresponds to protons from $^6\mathrm{Li}(d, p_0)^7\mathrm{Li}$. An energy of 1000 keV seems to be appropriate for lithium isotope analysis since the ^{6}Li yield is the highest obtained. Nevertheless, the ^{7}Li peak must be treated with special care due to ^{14}N interference.

The best performance of the $^6\mathrm{Li(d,}\alpha)^4\mathrm{He}$ reaction can be achieved with deuterons at low energy due to the cross-section of the reaction decreasing as a linear function in the range of 600 keV-2000 keV, see Fig. 2.6. Using deuterons with energies in the range 700 keV-1100 keV, a study of the possibility for ^{6}Li measurements in a Li-bearing samples was performed, as can be seen in Fig. 4.9. The ^{7}Li and ^{6}Li content is represented by the peaks at 6.5 MeV and 9.2 MeV respectively. Preliminary results indicates that $E_d = 1000$ keV would be an appropriate energy for the study of different samples.

Since there may be other light elements such as boron, oxygen or fluorine in the samples, additional charged particles can be produced like protons and αs on top of the ones obtained from reactions with lithium isotopes. Fig. 4.10 c)

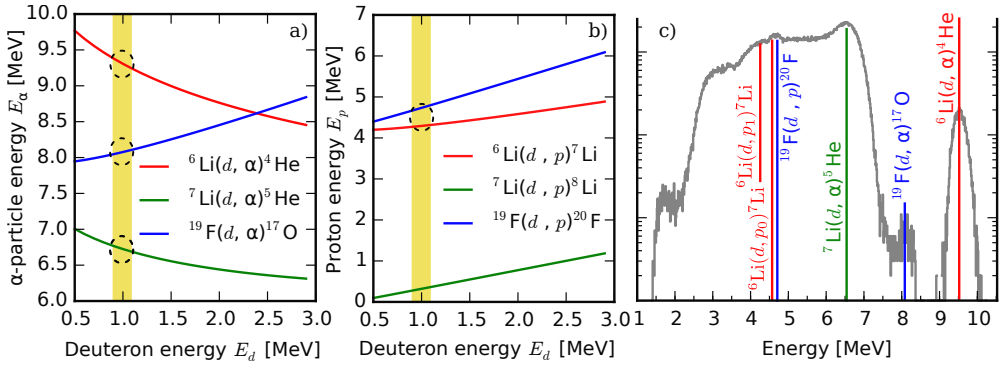

Figure 4.10: Possible energies of α particles a) and protons b) as a function of the deuteron energies (E_d) with a detection angle of 170°. The values are calculated based on kinematic equations when deuterons interact with ^{6}Li, ^{7}Li and ^{19}F. c) Experimental spectrum from a LiF glass scanned by a deuteron beam at 1000 keV.

shows the possible energy spectrum for the specific case of a LiF sample. In Figs. 4.10 a) and 4.10 b) it is shown the energies of α particles, a), and protons, b), as a function of the deuteron energies ,E_d. The energies were calculated at 170° for the case when the deuteron interacts with ^{6}Li, ^{7}Li, and ^{19}F leaving the recoil nucleus in the ground state. The yellow region marks the products at a beam energy of 1000 keV and the dotted circles highlight the reaction products also shown in c).

In the same spectrum (Fig. 4.10 c)) the origin of the peak around 2.0 MeV and part of the plateau between 3.0 MeV and 6.0 MeV can be explained by the overlap of protons produced in the ^{19}F$(d,p)^{20}$F and ^{6}Li$(d,p)^7$Li reactions[67]. Protons at 4.4 MeV and 4.7 MeV are emitted when the ^{20}F and ^{7}Li nuclei end up in their ground states. However, protons can also be emitted leaving the ^{20}F and ^{7}Li nuclei in excited states. These protons produce the peak around 2.0 MeV and the continuous distribution ranging from 2.5 MeV to 5.0 MeV.

The higher energy part of the plateau is produced from a similar situation as the lower energy side but for α particles instead of protons. From the plateau, a peak at 6.7 MeV from the ^{7}Li(d, α)^{5}He can be seen. In principle there should be another peak at 7.5 MeV from ^{19}F(d,α_1)^{17}O but its cross section is very small [2].

Finally, the peaks at 8.0 MeV and at 9.2 MeV are formed by α particles emitted from the ^{19}F$(d,\alpha)^{17}$O and ^{6}Li$(d,\alpha)^4$He reactions respectively. Both peaks are well-defined, and therefore are suitable for the extraction of ^{19}F and ^{6}Li concentrations.

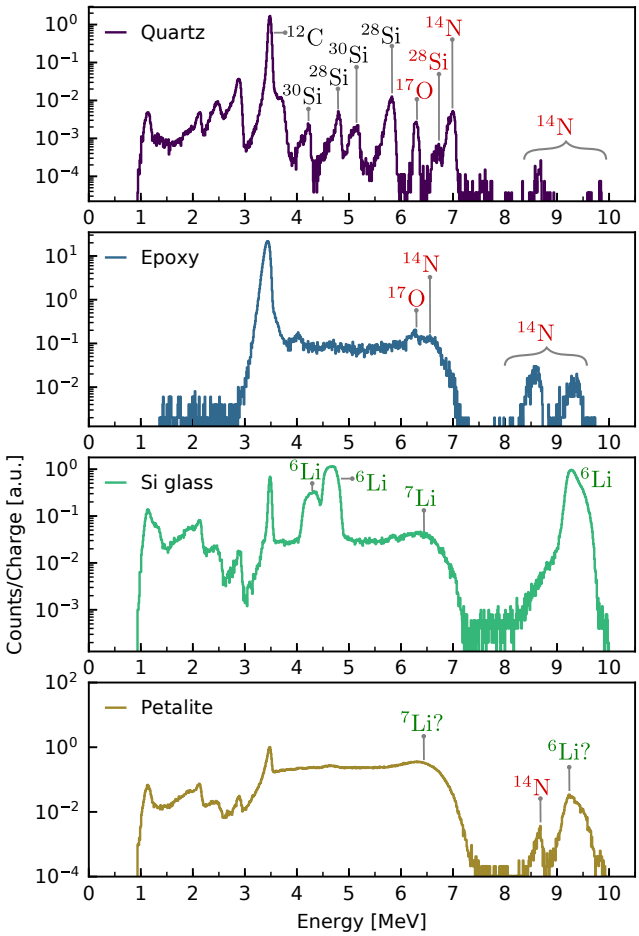

Figure 4.11: Energy spectra from synthetic (Quartz, Epoxy, Si glass detector) and natural (Petalite $LiAl(Si_4O_{10})$ samples scanned by a deuteron beam at 1000 keV.

Background contributions were investigated with deuterons at 1000 keV by scanning a set of samples, with and without lithium in them, and Fig. 4.9 shows the resulting spectra. It seems that a nitrogen interference for the ^{6}Li and ^{7}Li peaks is present. Additional interferences for ^{7}Li may come from oxygen and silicon. These results suggest the need for further experiments to optimize a method for ^{7}Li analysis. Once this difficulty has been overcome, it should be possible to quantify the different lithium isotopes in samples such as the silicon glass and the Petalite.

In the silicon glass spectrum it is noticeable that the high-energy ^{6}Li peak is significantly higher than the ^{7}Li one, this can be easily understood since the silicon glass is a detector doped with ^{6}Li. The Petalite, on the other hand, is a natural material and follows the expected ^{7}Li/ ^{6}Li ratio of 12.17%.

Since the samples are carbon coated to prevent them from being electrically charged, deuteron reactions with carbon took place as well. For instance, the sharp peak at $\sim$ 3 MeV in all the spectra in Fig. 4.9 is caused by the $^{12}\mathrm{C}(d, p_0)^{13}\mathrm{C}$ reaction. Counts in the carbon peak may also come from the sample itself since the minerals are embedded in epoxy which contains carbon and oxygen among other elements.

In the epoxy spectrum, peaks at $\sim$6.5 MeV, $\sim$8.5 MeV and $\sim$9.2 MeV come from the $^{14}\mathrm{N}(d, \alpha_1)^{12}\mathrm{C}$, $^{14}\mathrm{N}(d, p_0)^{15}\mathrm{N}$, and $^{14}\mathrm{N}(d, \alpha_0)^{12}\mathrm{C}$ reactions respectively. The peak at $\sim$8.5 MeV is also in the Petalite spectrum, which demonstrates the presence of nitrogen in the sample. This can be explained with epoxy remains on it.

Signals from ^{14}N represent an interference when extracting ^{7}Li and ^{6}Li yields at $\sim$6.5 MeV and $\sim$9.2 MeV respectively. Fortunately the $\sim$8.5 MeV peak is free from interference with lithium yield determination. The interference for ^{14}N in the samples can be accounted for by finding the total counts from the nitrogen peaks at 6.5 MeV (N_1), 8.5 MeV (N_2), and 9.2 MeV (N_3) from a pure epoxy spectrum and so determining the ratios N_2/N_3 and N_2/N_1. Using this ratios the nitrogen contribution to the ^{7}Li and ^{6}Li yields can be determined and subtracted.

5 DETERMINING FLUORINE CONTENT

In nature, fluorine is found as a single isotope with 9 protons and 10 neutrons. Its electronic configuration makes it the most reactive element in the periodic table [68]. Commonly, fluorine is not free, instead, fluorine forms compounds called fluorides. A large number of minerals contain fluorine as a primary constituent or include it as an impurity. Among primary minerals, tourmaline and fluorapatite contain low concentration of fluorine 1 wt% and ∼3.8 wt% respectively [69], while the content of fluorine is higher in fluorite and cryolite with concentrations of 48 wt% and 54 wt% respectively [70].

Fluorine with its 19 nucleons is considered a light element that can be quantified using NRA. The nuclear reactions extensively used for fluorine analysis are initiated by protons, deuteron and α particles [71]. Some Q-values for these reactions are listed in Table 1, their magnitudes are rather large which typically allows for easy detection.

The ^{19}F(p,α)^{16}O reaction was used for fluorine quantification. The reaction ^{19}F(d,α)^{17}O could be merely used to determine the presence of fluorine in the samples.

5.1 PROTON-INDUCED NUCLEAR REACTIONS ON F-BEARING MATERIALS

The interaction between a proton a fluorine atom leads to different mechanisms, such as Coulomb Excitation (^{19}F(p,p$_{1-5}\gamma$)^{19}F), Resonant Scattering (^{19}F(p, p)^{19}F) and nuclear reactions ((p,α), $(p,\alpha\gamma)$ (p,n)) [13]. In the case of nuclear reactions, the proton fuses with the fluorine nuclei, forming ^{20}Ne at a highly excitation energy. This excited compound nucleus, ^{20}Ne*, may de-excite via γ-rays emission or α-decay into ^{16}O. A simplified sketch of this process is shown in Fig. 5.1. The formation of ^{20}Ne and its α decay, ^{19}F(p, α)^{16}O, is of great importance and it was used in Paper IV to obtain the fluorine content in geological samples.

Quantification of fluorine through the $^{19}F(p, \alpha)^{16}O$ reaction

As was mentioned in the previous section, in this reaction the compound nucleus, ^{20}Ne, can α decay into ^{16}O, this process may leave the ^{16}O nucleus at

different excited states. The energy of the α particles emitted in this process depends on the initial and final energy states of ^{20}Ne and ^{16}O [13]. The decay into the ground state of ^{16}O defines a set of α particles, α_0, and so on for the another excited states defining other sets of α particles, α_i, see Fig. 5.1. In total, there are five groups of emitted α particles, that are commonly used for fluorine quantification. In this work only the first group was used since this group involves the highest possible energies which are convenient for identification and subsequently quantification. Throughout this chapter α_0 will be referred as α.

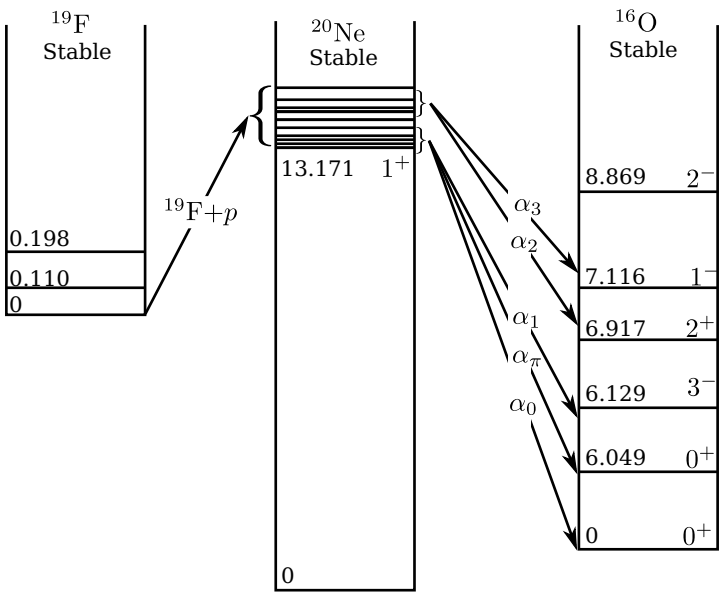

Figure 5.1: Simplified description of the ^{19}F(p, α)^{16}O process. Energy levels are not to scale and are indicated in MeV. Information taken from Refs [13, 14].

The cross-section for α emission is shown in Fig 2.6. In the region of low beam energies, ~800 keV, some small resonances are found whereas at higher energies, from 1300 keV to 1900 keV, much larger resonances are present. According to Ref. [31] the most convenient proton energy to carry out fluorine analysis is 1260 keV, due to the cross section remaining flat down to 1100 keV; within this energy range where the cross section is approximately constant there are not supposed to be interfering reactions. However, in this work it was found that for fluorine quantification studies, the ^{19}F(p,α)^{16}O reaction presented interference with α particles from the ^{7}Li(p, α)^{4}He reaction in Li-bearing samples, see Fig 5.2. The way to remedy this interference is to perform

the $^{19}F(p,\alpha)^{16}O$ reaction at lower energy. Paper I demonstrates the process of selecting an adequate proton energy in order to circumvent this.

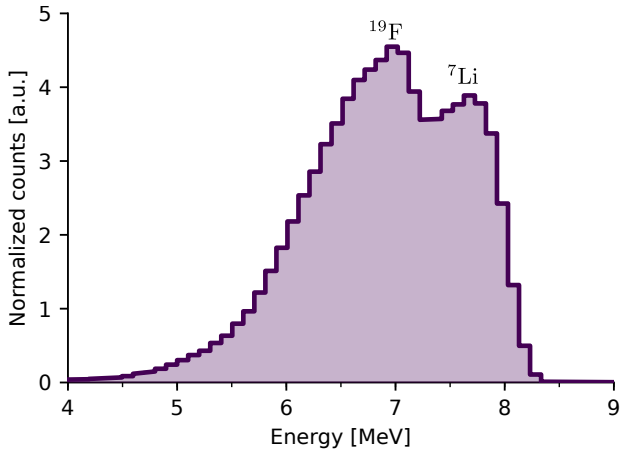

Figure 5.2: Energy spectrum from a LiF sample scanned with protons at 1200 keV for 10 minutes at a beam current of 3 nA. The ^{19}F and ^{7}Li signals clearly overlap.

In this work, proton energies ranging from 850 keV to 2000 keV were used to study the $^{19}F(p, \alpha)^{16}O$ reaction in the samples. This energy scan was performed to optimize fluorine analysis when interfering reactions may or may not arise. An energy of 850 keV was determined to be the most advantageous for fluorine analysis in Li-bearing samples.

A typical experimental spectrum from a thick CaF_2 sample is exhibited in Fig. 5.3 Left, this spectrum was produced when the sample was scanned with protons at 2000 keV for 10 minutes as part of the experiments presented in Paper IV. Since the sample is thick, the energies of the incoming protons and produced α particles decrease as a function of the depth in the sample. Due to the continue energy loss by the impinging protons in the sample, different resonances can arise. Those resonances are noticeable in the right side of Fig. 5.3 where simulated spectra from a CaF_2 sample with different thicknesses are shown. The thicker the sample, the more spread are the energies of the α particles coming from the $^{19}F(p, \alpha)^{16}O$ reaction. The experimental spectrum is very similar to the simulated spectrum from the thickest simulated sample.

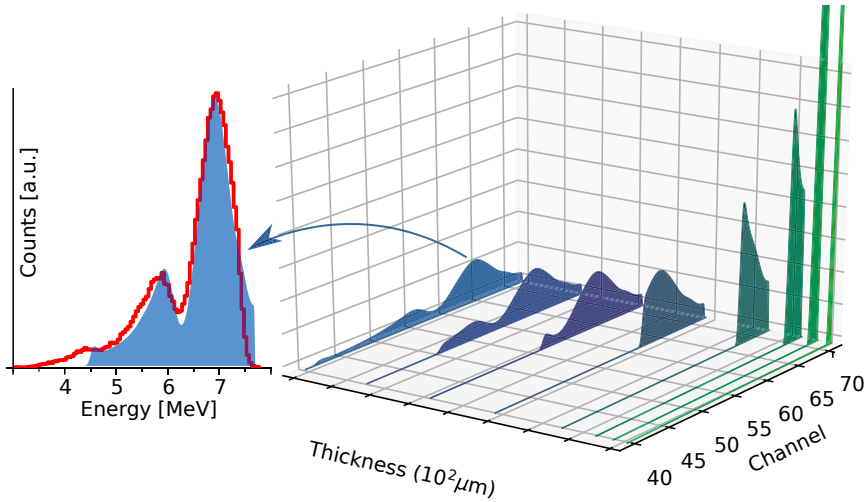

Figure 5.3: Left: In red a typical experimental spectrum from a CaF_2 sample scanned with a proton beam at 2000 keV for 10 minutes; in blue, a simulated spectrum is presented for comparison. Right: various simulated spectra from CaF_2 samples of different thicknesses. Results simulated with SIMNRA [15].

5.2 DEUTERON-INDUCED NUCLEAR REACTIONS ON F-BEARING MATERIALS

The use of deuteron beams is suitable when fluorine is determined simultaneously with light elements such as ^{6}Li, ^{9}Be,^{12}C, ^{16}O, which cannot be measured using proton-induced reactions. If this is not the case, proton induced reaction is preferred to perform the nuclear microanalysis of fluorine [2].

Deuteron-induced nuclear reactions on F-bearing materials can lead to the creation of protons and α particles. In the experiments performed for preliminary reported in Chapter 4, α particles from the ^{19}F(d,α)^{17}O reaction were detected for a LiF and a CaF_2 sample. Fig. 4.10 shows the α particles from this reaction.

It should be stated that no fluorine quantification was done in this study since proton-induced methods produce cleaner spectra which are easier to analyze and do not contain interference from other elements besides lithium. Fortunately, the lithium interference is easily accounted for when an adequate beam energy is selected.

6

SUMMARY AND OUTLOOK

The investigation of the content of lithium and fluorine isotopes in geological samples using NRA has shown that the proton and deuteron-induced α-emission reactions give well-separated and clean signals under certain conditions that are related to the parameters under which the reactions take place and the chemical composition of the samples. For that reason, the reactions were studied at different ion energies using geological samples with variations in lithium and fluorine concentrations.

These reactions were chosen due to their reasonably good cross sections and high reaction Q-values which, combined with the possibility of performing the reactions at high beam current, allowed to measure ^{7}Li and ^{19}F concentration below 1 ppm and 50 ppm respectively. These results contribute to the expansion of the capabilities of measuring light elements at LIBAF.

The present study demonstrates that the $^{19}\mathrm{F}(p,\alpha)^{16}\mathrm{O}$ and $^{7}\mathrm{Li}(\mathrm{p},\alpha)^{4}\mathrm{He}$ reactions initiated by protons at about 800 keV produce two α-particle distributions, corresponding to the ^{19}F and ^{7}Li presences. The peaks are easily distinguishable on the background-free energy spectrum. Thus, the simultaneous analysis of ^{7}Li and ^{19}F seems to be advantageous using protons at about 800 keV. The use of this energy also induces reactions with other light elements such as boron, nitrogen, and oxygen, however they do not represent any risk of interference with fluorine either lithium. When the reactions were initiated by protons at higher energies, the distributions corresponding to ^{7}Li and ^{19}F begin to overlap.

The $^{7}\mathrm{Li}(d,\alpha)^{5}\mathrm{He}$ and $^{6}\mathrm{Li}(d,\alpha)^{4}\mathrm{He}$ reactions were utilized to investigate isotopes of lithium with deuteron energies from 700 keV to 1100 keV. It was found that an energy of 1000 keV seems to be appropriate for lithium isotopes analysis since ^{6}Li yield is the highest obtained. Nevertheless, the ^{7}Li peak must be treated with special care due to interference from oxygen, silicon and nitrogen. These results suggest the need for further experiments to optimize a method for ^{7}Li analysis using deuteron-induced reactions.

Nitrogen analysis will be possible to perform since signals from the reactions such as $^{14}\mathrm{N}(d,p_0)^{15}\mathrm{N}$, $^{14}\mathrm{N}(d,\alpha_0)^{12}\mathrm{C}$ and $^{14}\mathrm{N}(d,\alpha_1)^{12}\mathrm{C}$ could be identified using deuterons at 1000 keV.

Thanks to the use of PIXE as a complementary technique of NRA, light and heavy elements were detected simultaneously, so 2D-distribution maps of elements such as iron were obtained. The mapping results in geological samples showed compositional zoning. As a continuation of this study, a quantitative PIXE analysis of samples with well-known composition should be done.

The findings shown in this thesis were acquired thanks to a huge effort of the group at LIBAF to construct the new Total IBA chamber and to develop a charged-particle detection system that counts with a DSSSD. The implementation of this segmented detector gave the possibility of performing NRA at high beam current, since the use of the DSSSD reduced notably the pile up effect.

The DSSSD geometry could also be utilized for measuring cross-section measurements of other reactions.

Simulation of the DSSSD could help to understand in more details the spectra from thick samples using NRA. A fit of a spectrum and the final yield of the elements of interest can be determined by the simulation.

ACKNOWLEDGMENT

This thesis was possible thanks to the effort and support from many people. Among them is my main supervisor, Charlotta Nilsson, who gave me the opportunity to enroll in the Ion Beam Analysis research. My co-supervisor Robert Frost, who designed the new beam deflector controller, without this device, all the work done in Paper IV would end in several pointless histograms. My previous co-supervisors, Per Kristiansson, who never really stopped being my supervisor, and Linus Ros, who introduced me to the job of using the tailored 200 parameter VME-based data acquisition system for IBA at LIBAF.

I would also like to thank Jan Pallon, Mikael Elfman and Mikael Elkholm, members of the group at LIBAF, for helping and guiding me at the laboratory.

I would like to thank the people at the Division of Nuclear Physics who have supported me during my PhD. Dirk Rudolph for driving the Division. Göran Frank for supporting me with my PhD program. Pavel Golubev helping me understanding the physics of the DSSSD, among other things.

The atmosphere at the Division has been fantastic thanks to Emil, Moa, Ulrika, Oscar, Anton, Markus, Alex, Nicholai, Johan, Danny, Frame, Guilllaume, Vytenis, Jason among other members.

Thank you very much to my family and my friends for always being with a positive attitude when I was being a pessimist.

Jamás hubiera culminado un trabajo como este sin el espíritu luchador que mi querida madre Alba me inculcó. Por eso y por un billon de motivos más, muchas gracias mamita.

Y a mi Pico favorito que está sobrelapado conmigo ¡GRACIAS TOTALES!

REFERENCES

[1] National Institute of Standards and Technology. *Certificate*. https://www-s.nist.gov/srmors/certificates/610.pdf. Accessed:2017-11-17.

[2] B. Maurel, et al. Nuclear Instruments and Methods in Physics Research, **191(1)**, 349 – 356 (1981).

[3] D. Dieumegard, et al. Nuclear Instruments and Methods, **168(1)**, 93 – 103 (1980).

[4] J.M.Delbrouck-Habaru, et al. Jour. Bull.Societe Royale des Sciences de Liege, **38**, 240 (1969).

[5] International Atomic Energy Agency. *Ion Beam Analysis Nuclear Data Library*. https://www-nds.iaea.org/exfor/ibandl.htm. Accessed:2019-04-26.

[6] National Electrostatic Corp. *Introduction Manual for Installation, Operation, and Maintenance, High Pressure Environment, Positive Ion R.G. Source*. NEC (1990).

[7] A. Shariff, et al. Nuclear Instruments and Methods in Physics Research Section B, **231(1-4)**, 7–13 (2005).

[8] KETEK. *AXAS-M Modular system with VITUS SDD and reset type low-noise preamplifier in thermally optimized AXAS-M1 housing*. https://http://www.ketek.net/sdd/complete-systems/axas-m/. Accessed:2019-05-08.

[9] P. Golubev, et al. Nuclear Instruments and Methods in Physics Research Section B: Beam Interactions with Materials and Atoms, **267(12-13)**, 2065–2068 (2009).

[10] M. Natasi, et al. *Ion Beam Materials Analysis, Fundamentals and Applications*. CRC Press, Boca Raton, FL (2015).

[11] N. De La Rosa, P. Kristiansson, E. J. C. Nilsson, L. Ros, M. Elfman, J. Pallon. Nuclear Instruments and Methods in Physics Research Section B: Beam Interactions with Materials and Atoms, **404**, 29–33 (2017).

[12] M. Elfman, et al. Nuclear Instruments and Methods in Physics Research Section B, **231(1-4)**, 14–20 (2005).

[13] J. W. J.R Bird. *Ion Beams for Materials Analysis.* Academic Press, Sydney (1989).

[14] P. Cabanelas et al. Nuclear Instruments and Methods in Physics Research Section B: Beam Interactions with Materials and Atoms, **381**, 110 – 113 (2016).

[15] M. Mayer. *SIMNRA, Computer simulation of RBS, ERDA, NRA, MEIS and PIGE*. http://home.mpcdf.mpg.de/~mam/. Accessed: 2019-05-16.

[16] P. Kristiansson. *Tailored techniques for isotope analysis in geoscience by ion beam microscopy*. Project Research Grant: 2014-3916-115737-49. The Swedish Research Council-Vetenskapsrådet (2014).

[17] P. Kristiansson, et al. Nuclear Instruments and Methods in Physics Research Section B: Beam Interactions with Materials and Atoms, **306**, 253 – 256 (2013).

[18] M. Borysiuk, et al. Nuclear Instruments and Methods in Physics Research Section B: Beam Interactions with Materials and Atoms, **306**, 49 – 53 (2013).

[19] M. Borysiuk, et al. Nuclear Instruments and Methods in Physics Research Section B: Beam Interactions with Materials and Atoms, **269(20)**, 2229 – 2232 (2011).

[20] P. Kristiansson, et al. Nuclear Instruments and Methods in Physics Research Section B: Beam Interactions with Materials and Atoms, **332**, 207 – 211 (2014).

[21] E. J. C. Nilsson, et al. Journal of Radioanalytical and Nuclear Chemistry, **311(1)**, 355–364 (2017).

[22] D. Mota de Freitas, et al. Met. Ions Life Sci., **16(1)**, 557 –584 (2016).

[23] G. Coote. Nuclear Instruments and Methods in Physics Research Section B: Beam Interactions with Materials and Atoms, **66(1)**, 191 – 204 (1992).

[24] S. Radhakrishnan, et al. Science Advances, **3(7)**, e1700 842 (2017).

[25] M. Wu, C. Cao, J. Jiang. Nanotechnology, **21(50)**, 505 202 (2010).

[26] M. Roberge, et al. Earth and Planetary Science Letters, **429**, 25 – 32 (2015).

[27] K. T. Koga et al. Comptes Rendus Chimie, **21(8)**, 749 – 756 (2018).

[28] S. Rio, et al. Nuclear Instruments and Methods in Physics Research Section B: Beam Interactions with Materials and Atoms, **100(1)**, 141 – 148 (1995).

[29] F. Watt et al. *Principles and applications of high-energy ion microbeams*. Adam Hilger, Bristol (1987).

[30] K. L. Linge, et al. Geostandards and Geoanalytical Research, **41(4)**, 493–562 (2017).

[31] Y. Wang et al. *Handbook of Modern Ion Beam Materials Analysis*, vol. 1. 2nd ed. Materials Research Society (2009).

[32] N. De La Rosa. *Nuclear Reaction Analysis in Li-bearing samples*. Licentiate Thesis, Lund University, Lund, Sweden (2018).

[33] J. L. Campbell, et al. *Particle-induced X-ray emission spectrometry (PIXE).* Chemical analysis 133. New York , John Wiley and Sons, cop. (1995).

[34] T. Calligaro, et al. III Congreso Nacional de Aqueometría, Sevilla: Universidad de Sevilla, 198–206 (1999).

[35] G. W. Grime et al. *Beam Optics of Quadrupoles Probe-Forming Systems*. Adam Hilger, Bristol U.K (1984).

[36] K. G. Malmqvist. *Particle-Induced X-Ray Emission - A Quantitative Technique Suitable for Microanalysis*. Springer Vienna, Vienna (1996).

[37] K. Krane. *Introductory Nuclear Physics*. John Wiley & Sons, USA (1988).

[38] E. E. Ritter, et al. Nuclear Instruments and Methods in Physics Research Section B: Beam Interactions with Materials and Atoms, **407**, 47 – 54 (2017).

[39] R. Mateus, et al. Nuclear Instruments and Methods in Physics Research Section B: Beam Interactions with Materials and Atoms, **219-220**, 519 – 523 (2004).

[40] J. S. Lilley. *Nuclear physics : principles and applications.* The Manchester physics series. Chichester ; New York : J. Wiley (2001).

[41] W. R. Leo. In *Techniques for Nuclear and Particle Physics Experiments, A how to Approach*, 2nd ed., 278. Springer-Verlag, Germany (1994).

[42] J. F. Ziegler. *SRIM - The Stopping and Range of Ions in Matter*. https://http://www.srim.org/. Accessed:2019-04-26.

[43] M. Kokkoris. *Nuclear Reaction Analysis (NRA) and Particle-Induced Gamma-Ray Emission (PIGE)*, chap. Ion Beam Techniques, 1–18. American Cancer Society (2012).

[44] G. Amsel et al. Ann. Rev. Nucl. Part. Sci., **34**, 435–460 (1984).

[45] A. Makishima. *Thermal ionization mass spectrometry (TIMS) : silicate digestion, separation, measurement.* Wiley-VCH (2016).

[46] R. Thomas. *Practical Guide to ICP-MS: A Tutorial for Beginners, Third Edition.* CRC Press (2013).

[47] M. S. Shackley. *An Introduction to X-Ray Fluorescence (XRF) Analysis in Archaeology*. Springer New York, New York, NY (2011).

[48] F. Watt, et al. *Principles and applications of high-energy ion microbeams.* Bristol Hilger (1987).

[49] S. A. E. Johansson et al. *PIXE : a novel technique for elemental analysis.* Chichester: Wiley, cop (1988).

[50] A. Shariff, et al. Nuclear Instruments and Methods in Physics Research Section B, **231(1)**, 1–6 (2005).

[51] National Electrostatic Corp. *Pelletron charging system*. http://www.pelletron.com/products/pelletron-charging-chains. Accessed: 2019-05-03.

[52] National Electrostatic Corp. *Introduction Manual for Operation and Service*. NEC (1990).

[53] P. Kristiansson, et al. Nuclear Instruments and Methods in Physics Research Section B: Beam Interactions with Materials and Atoms, **268(11-12)**, 1727–1730 (2010).

[54] Electronic Projects Components Available Worldwide. *Teensy usb development board*. https://www.pjrc.com/store/teensy32.html. Accessed:2019-10-11.

[55] M. Borysiuk, et al. Nuclear Instruments and Methods in Physics Research Section B: Beam Interactions with Materials and Atoms, **306**, 49–53 (2013).

[56] G. Lutz. In *Semiconductor Radiation Detectors,Device Physics*, 116. Springer, Munich, Germany (2007).

[57] International Atomic Energy Agency. *Live Chart of Nuclides*. https://www-nds.iaea.org/relnsd/vcharthtml/VChartHTML.html. Accessed:2018-02-02.

[58] KETEK. *SDD Working Principle*. https://http://www.ketek.net/sdd/technology/working-principle/. Accessed:2019-05-08.

[59] G. F. Knoll. *Radiation detection and measurement*. Wiley (2000).

[60] Mesytec. *Mprs-16 data sheet v1.4*. https://www.mesytec.com/products/datasheets/MPRS-16.pdf. Accessed:2018-05-07.

[61] M. Elfman, et al. Nuclear Instruments and Methods in Physics Research Section B: Beam Interactions with Materials and Atoms, **371**, 148 – 152 (2016).

[62] L. Ros. *A Detector System for Light-Element Analysis using Nuclear Microprobe for Application in Geoscience*. Ph.D. thesis, Lund University, Sweden (2016).

[63] Y. Gao, et al. Geochemistry, Geophysics, Geosystems, **13(10)**, 75–81 (2012).

[64] Y. Sunitha et al. Nuclear Instruments and Methods in Physics Research Section B: Beam Interactions with Materials and Atoms, **400**, 22 – 30 (2017).

[65] Eric Eason. *World Lithium Supply*. http://large.stanford.edu/courses/2010/ph240/eason2/. Accessed:2018-01-31.

[66] L. Chan. In P. A. d. Groot, ed., *Handbook of Stable Isotope Analytical Techniques*, 122 – 141. Elsevier, Amsterdam (2004).

[67] Y. Wang et al. *Handbook of Modern Ion Beam Materials Analysis, Appendices*, vol. 1. 2nd ed. Materials Research Society (2009).

[68] B. L. Fina et al. In *Fluorine: Chemistry, Analysis, Function and Effects*, 41–53. The Royal Society of Chemistry (2015).

[69] N. N. Greenwood et al. *Chemistry of the Elements.*, vol. 2nd ed. Butterworth-Heinemann (1997).

[70] M. G. García et al. In *Fluorine: Chemistry, Analysis, Function and Effects*, 3–21. The Royal Society of Chemistry (2015).

[71] G. Coote. Nuclear Instruments and Methods in Physics Research Section: B Beam Interactions with Materials and Atoms, **66(1)**, 191–204 (1992).

Part II

SCIENTIFIC PUBLICATIONS